Supporting Information for

Rhodamine 6G based efficient chemosensor for the trivalent metal ions (Al^{3+}, Cr^{3+} and Fe^{3+}) upon single excitation with applications in combinational logic circuits and memory devices

Dipankar Das[a] , Rabiul Alam[a] and Mahammad Ali[a,*]

[a]*Department of Chemistry, Jadavpur University, Kolkata 700 032, India, Fax: 91-33-2414-6223, E-mail: m_ali2062@yahoo.com,*

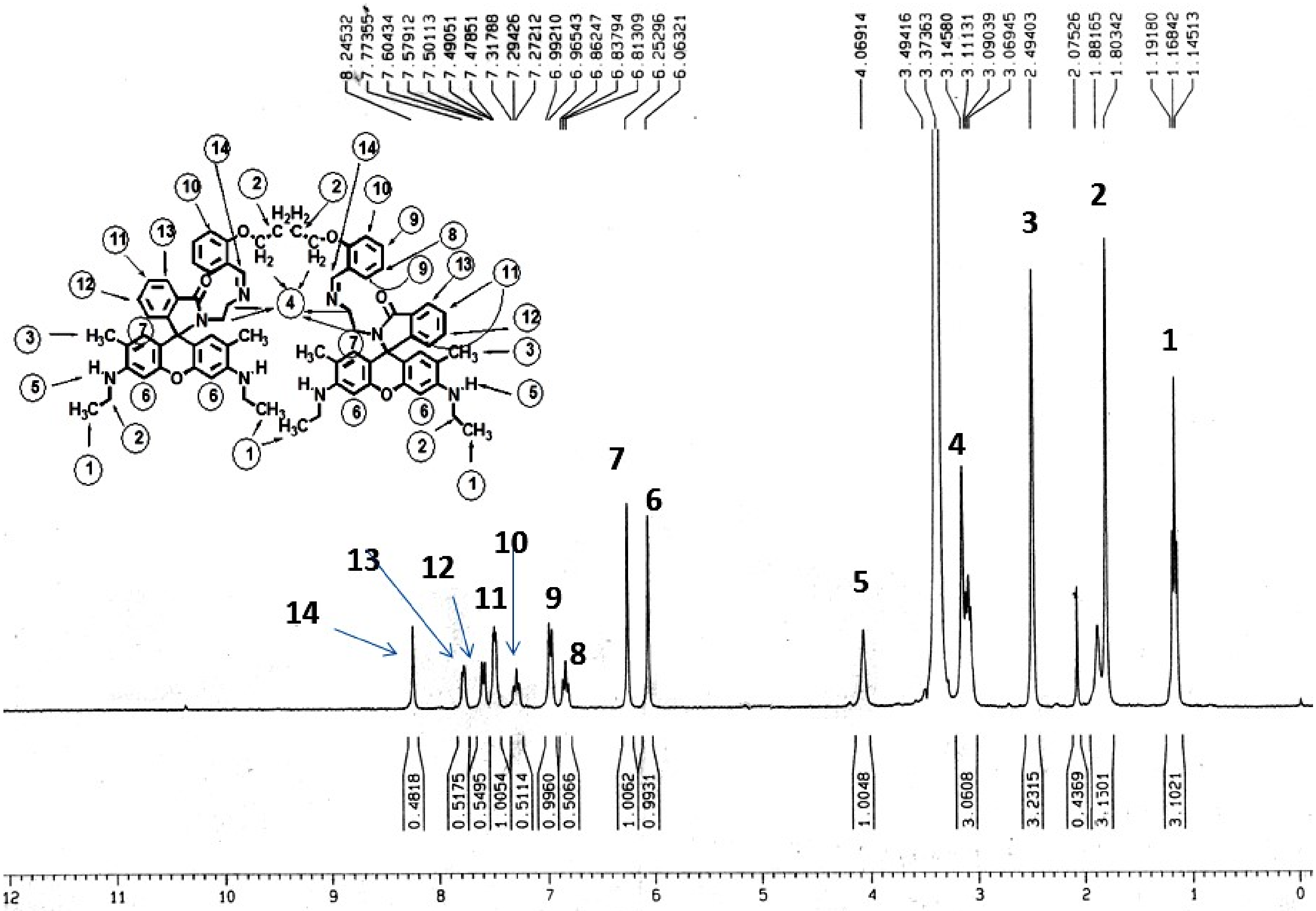

Fig. S1.^{1}H NMR spectrum of $\mathbf{L^3}$ in DMSO-d_6, in Bruker 300 MHz instrument.

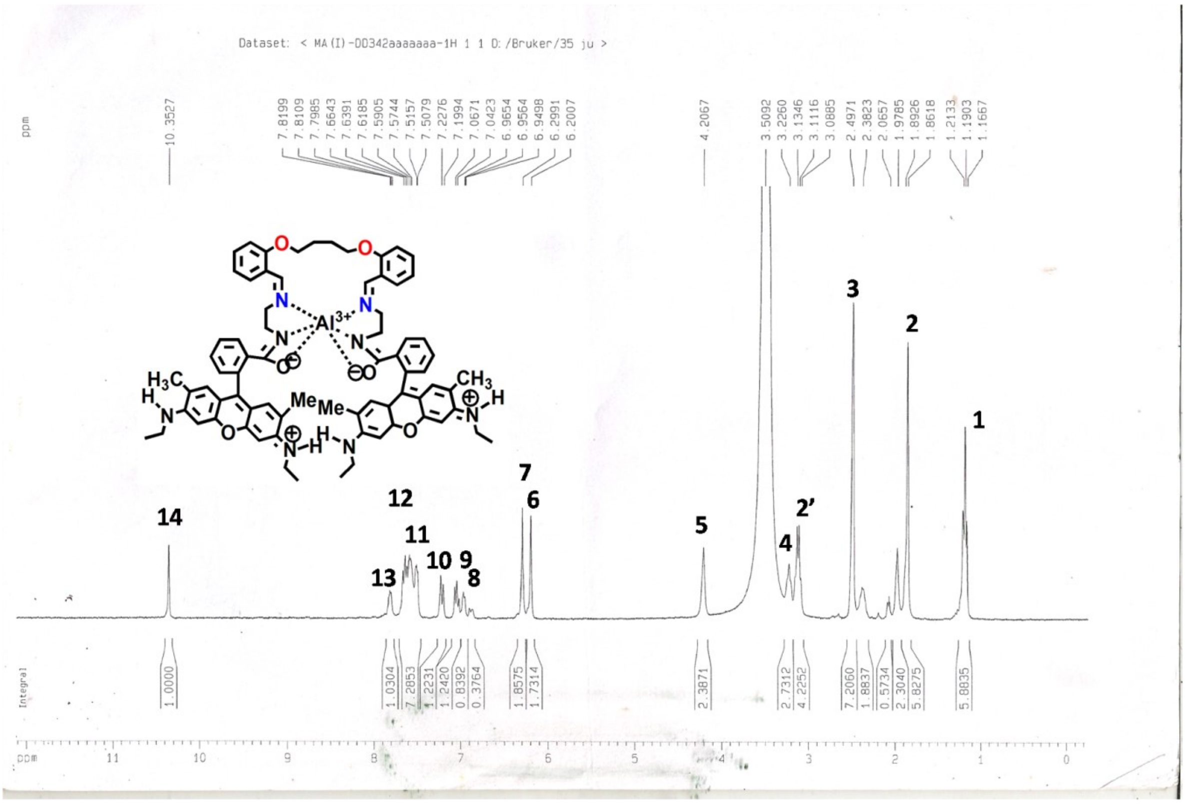

Fig. S1a.[1]H NMR spectrum of [**L**[3]-Al^{3+}]complex in DMSO-d_6, in Bruker 300 MHz instrument.

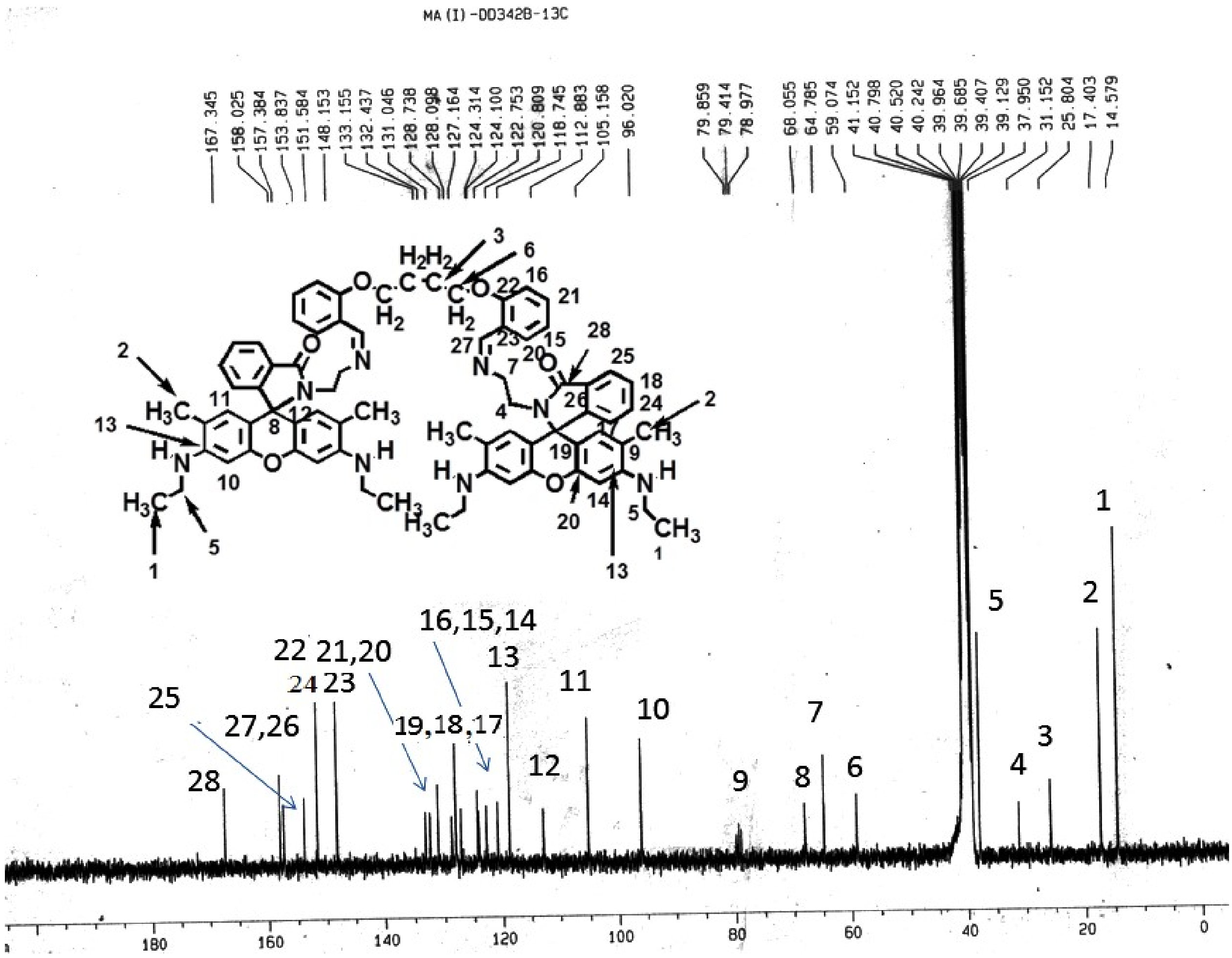

Fig. S2. ^{13}C NMR spectrum of $\mathbf{L^3}$ in DMSO-d_6, in Bruker 300 MHz instrument.

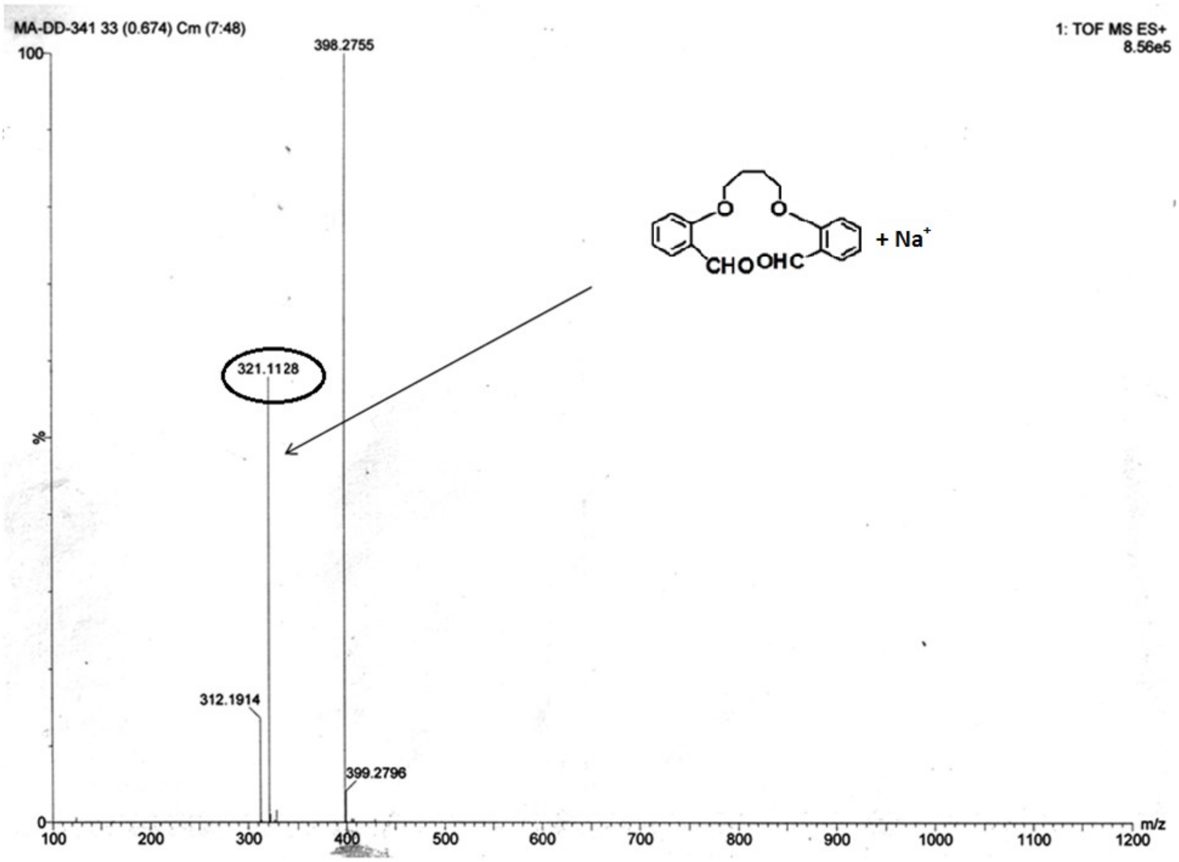

Fig.S3. Mass spectroscopy of $\mathbf{L^2}$ in MeCN.

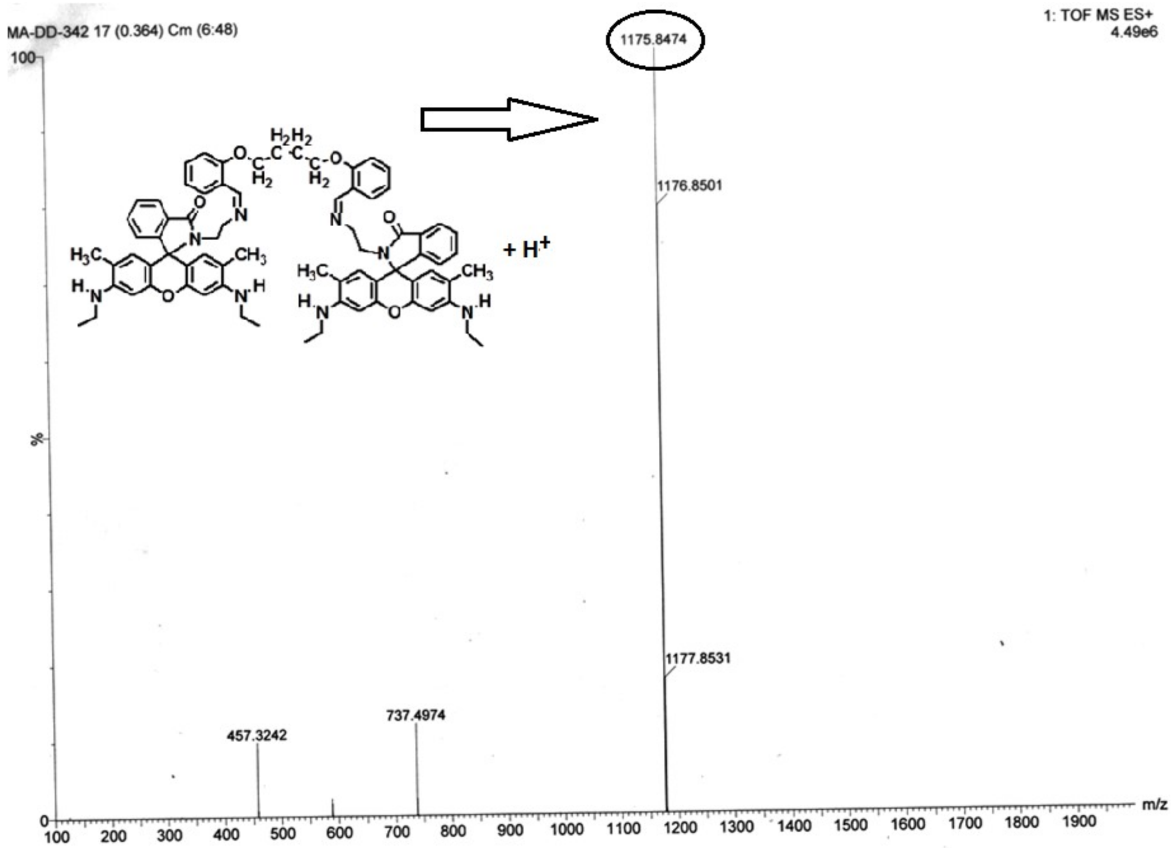

Fig. S3a. Mass spectroscopy of L^3 in MeCN.

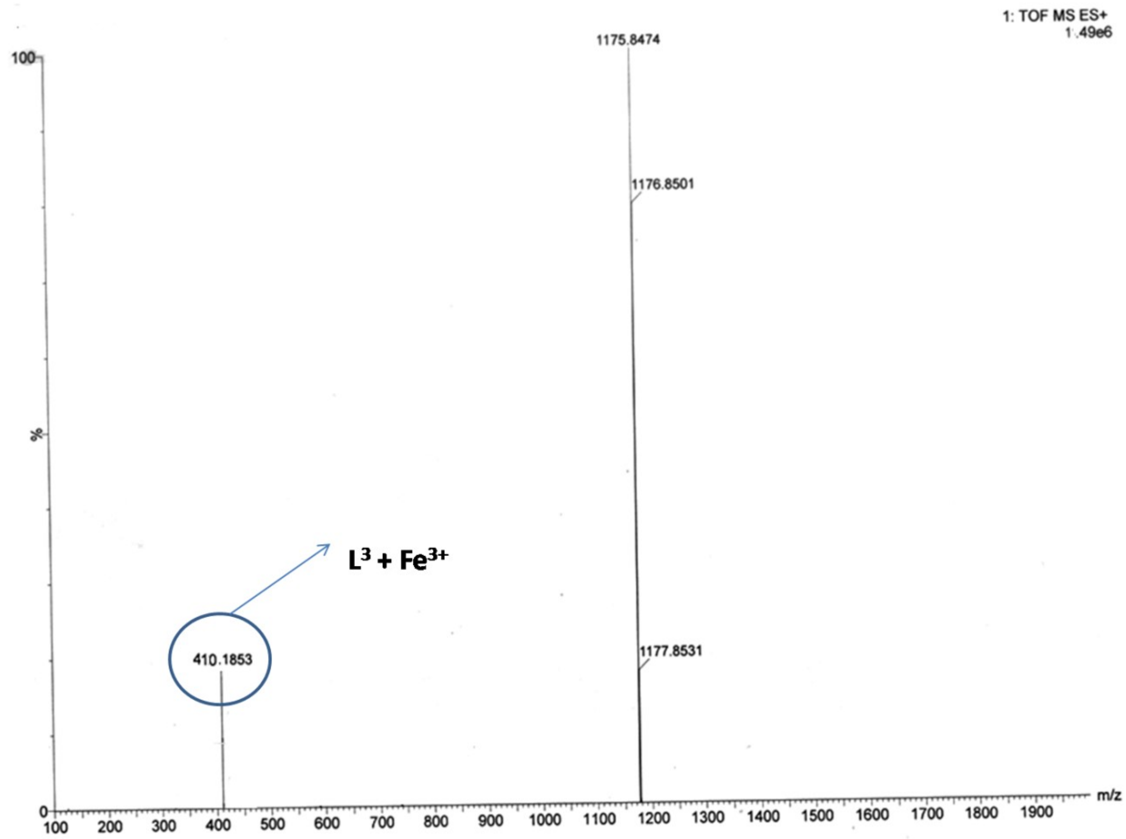

Fig. S3b. Mass spectroscopy of [$L^3 + Fe^{3+}$] in MeCN.

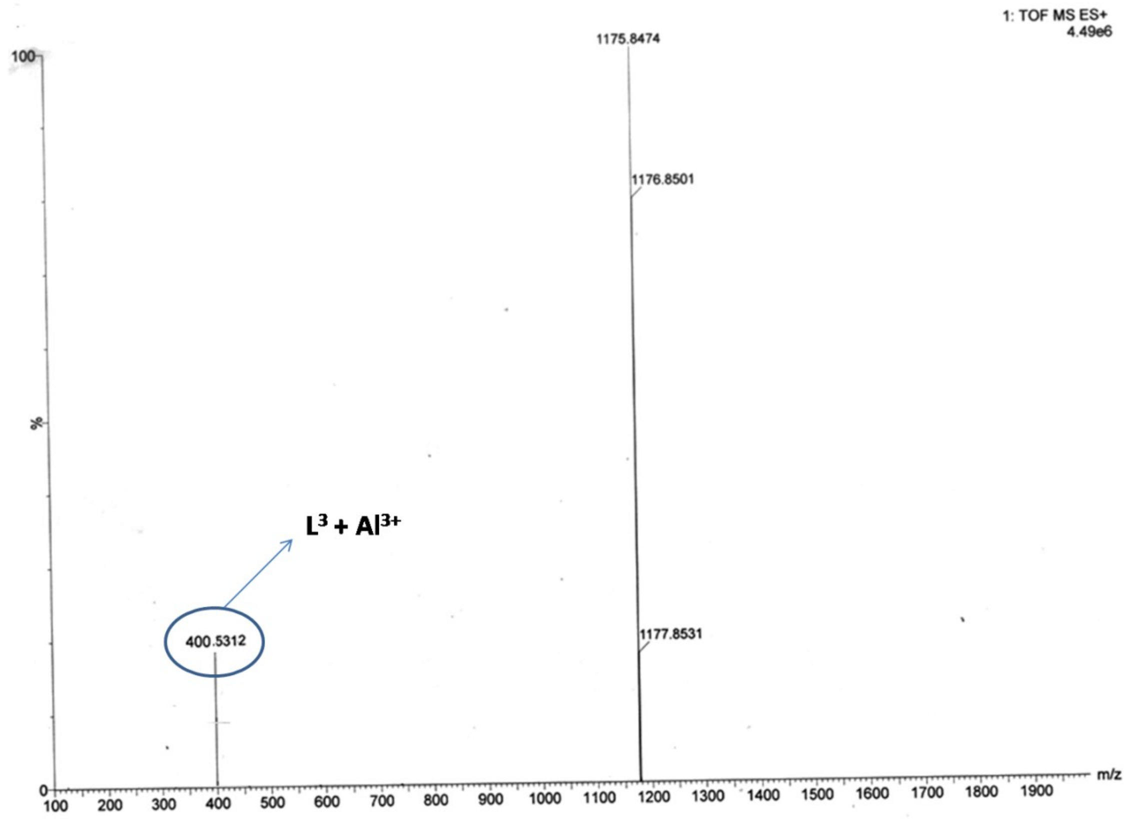

Fig. S3c. Mass spectroscopy of [L^3 + Al^{3+}] in MeCN.

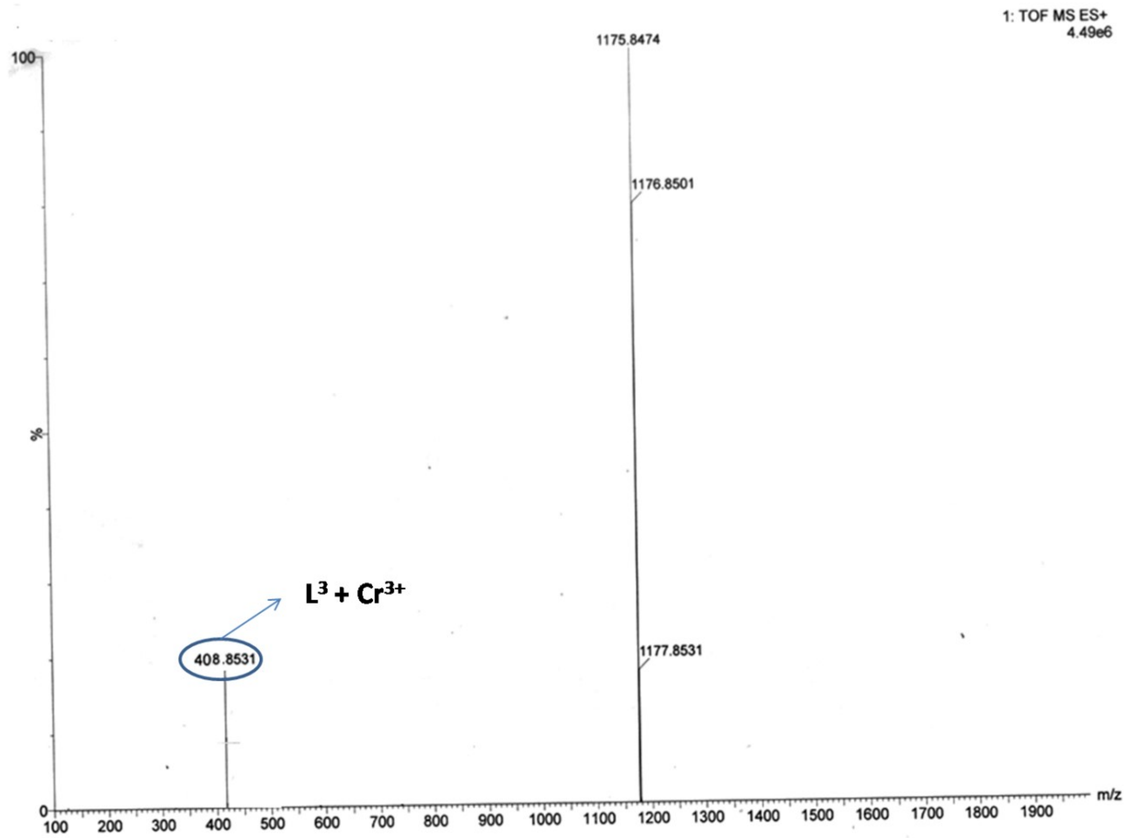

Fig. S3d. Mass spectroscopy of [$L^3 + Cr^{3+}$] in MeCN.

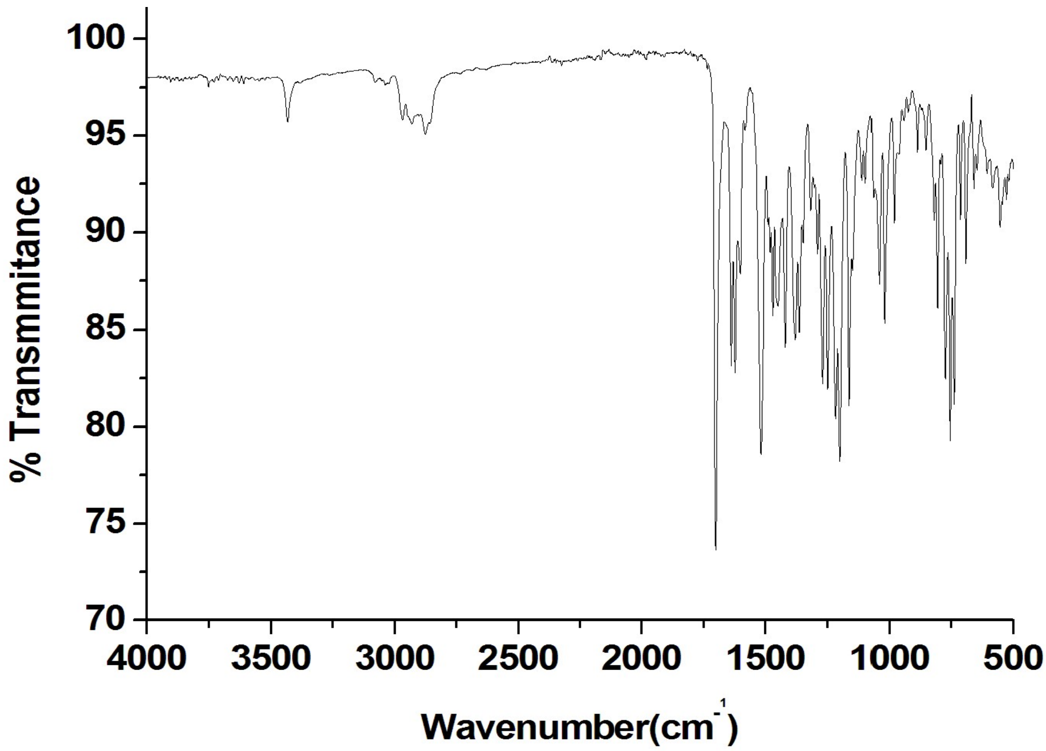

Fig. S4. FT-IR spectrum of $\mathbf{L^3}$

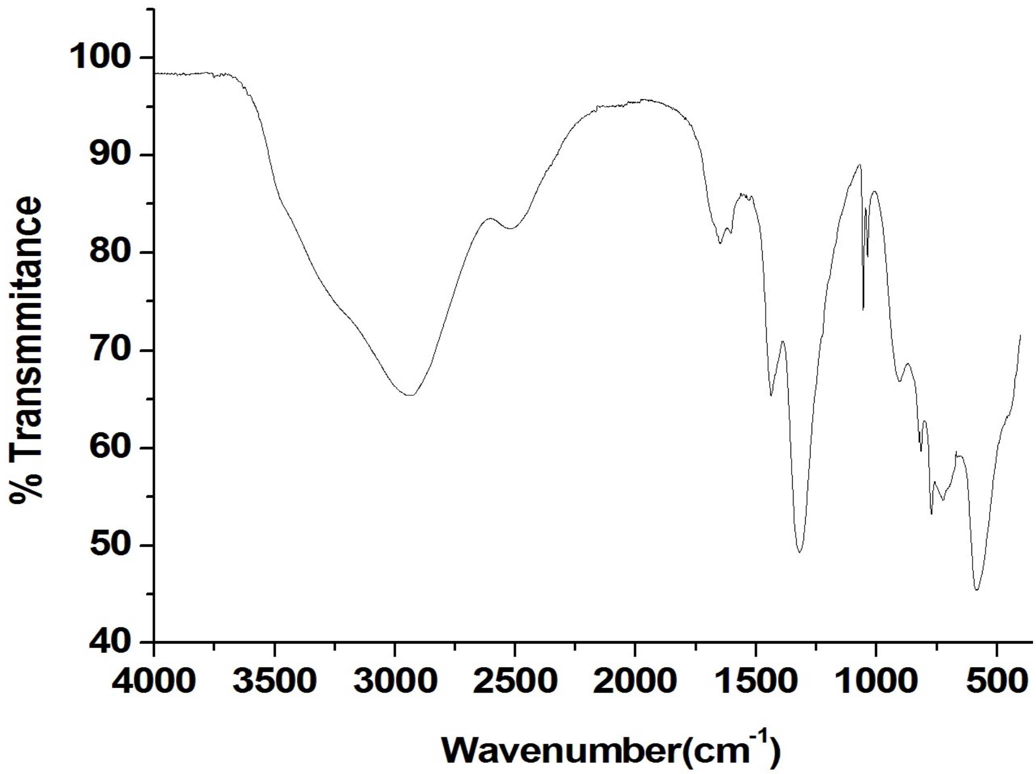

Fig. S4a. FT-IR spectrum of [$\mathbf{L^3}$+Al^{3+}] Complex.

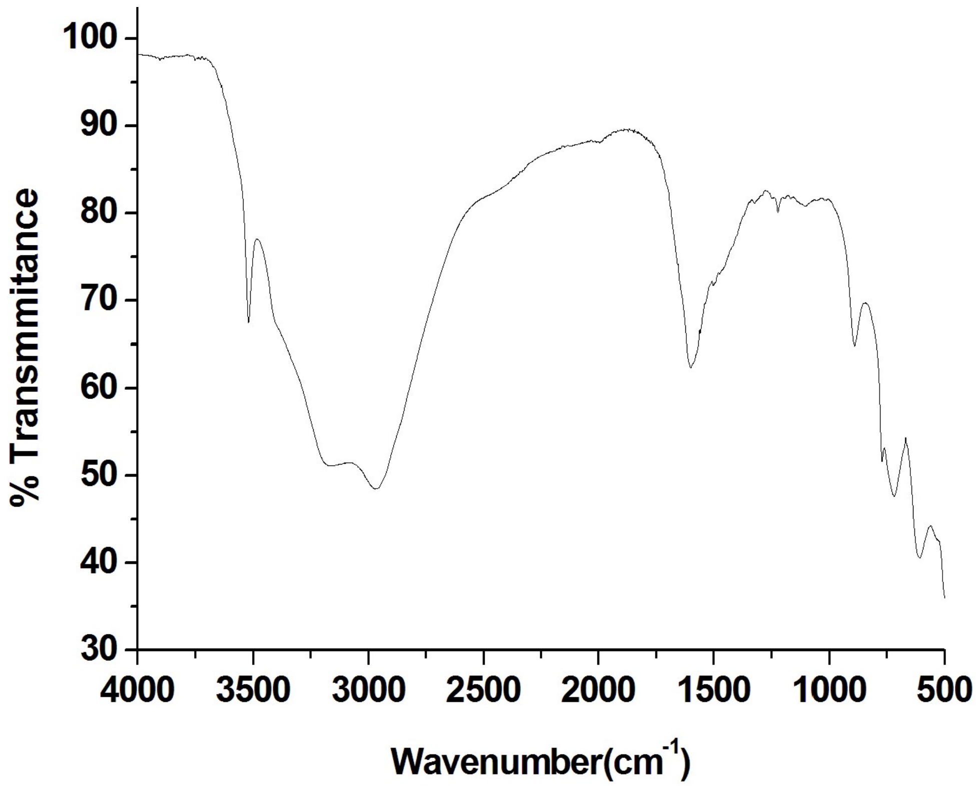

Fig. S4b. FT-IR spectrum of [**L**^{3}+Cr^{3+}]Complex.

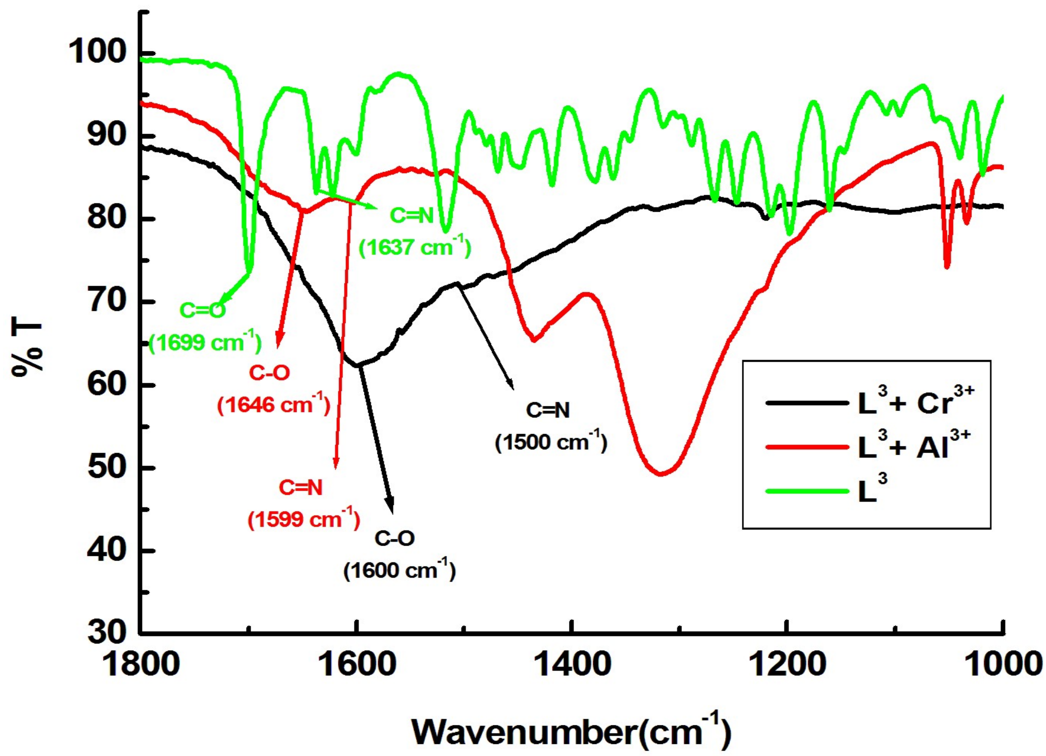

Fig.S4c. IR spectra of **(L**^{3}**), [L**^{3}**–Al**$^{3+}$] and[**L**^{3}**–Cr**$^{3+}$] complexes in MeCN.

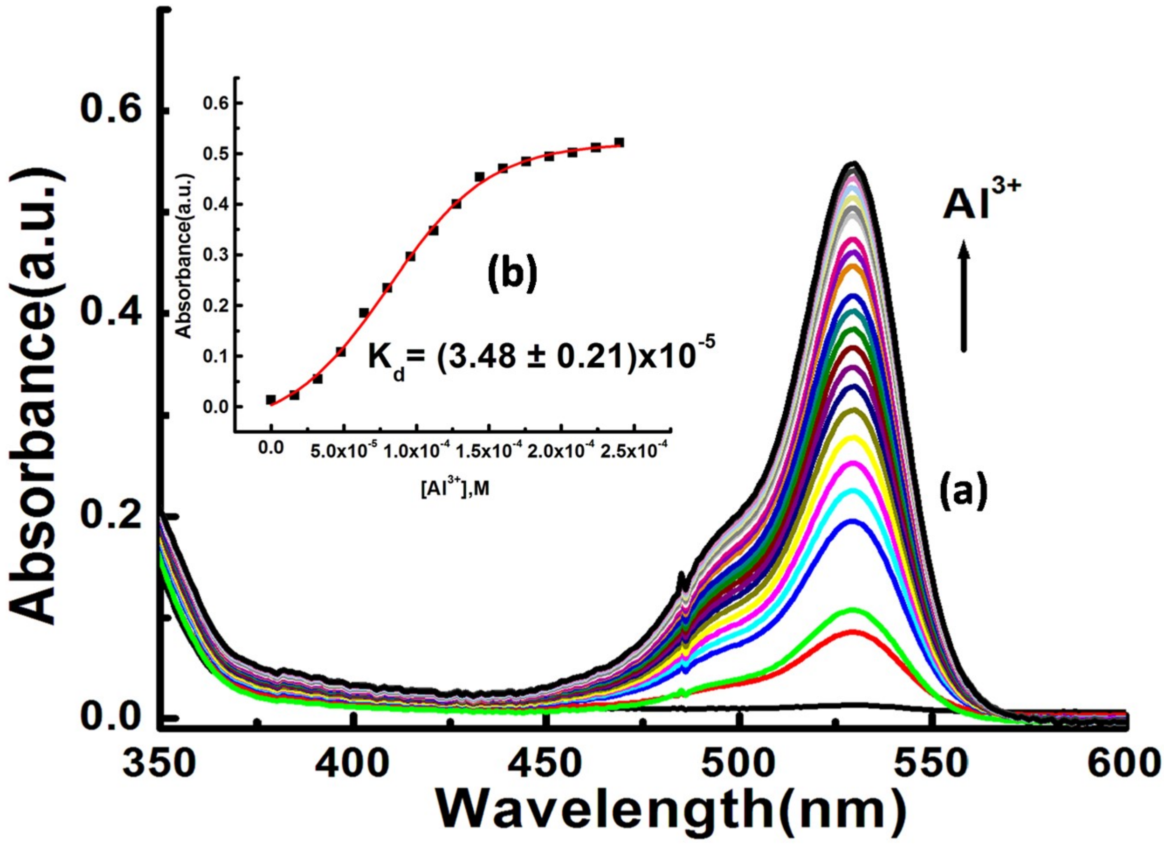

Fig. S5. (a) UV-VIS titration of **L^3**(60 μM) in H_2O- MeCN-(7:3, v/v) in HEPES buffer at pH 7.2 by the gradual addition of Al^{3+} (0-336 μM). Inset (b)Nonlinear curve-fit of F.I vs. [Al^{3+}] plot.

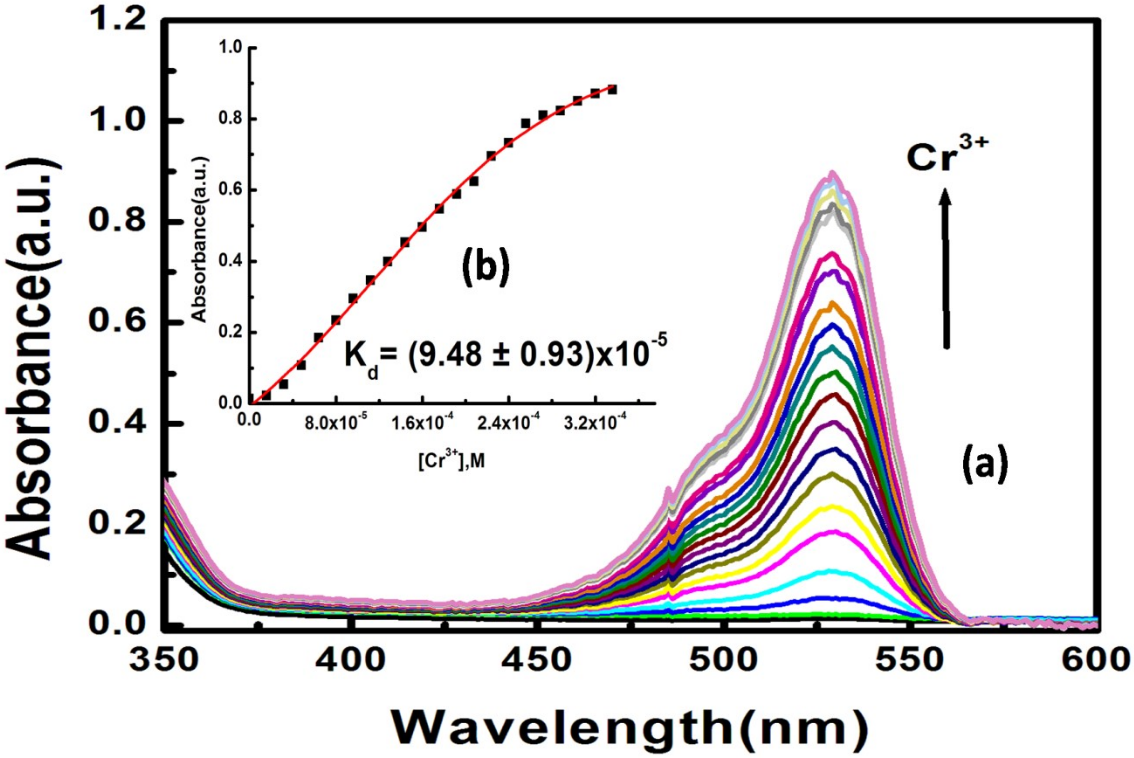

Fig. S5a. (a) UV-VIS titration of **L^3**(60 μM) in H_2O- MeCN-(7:3, v/v) in HEPES buffer at pH 7.2 by the gradual addition of Cr^{3+} (0-336 μM). Inset (b)Nonlinear curve-fit of F.I vs. [Cr^{3+}] plot.

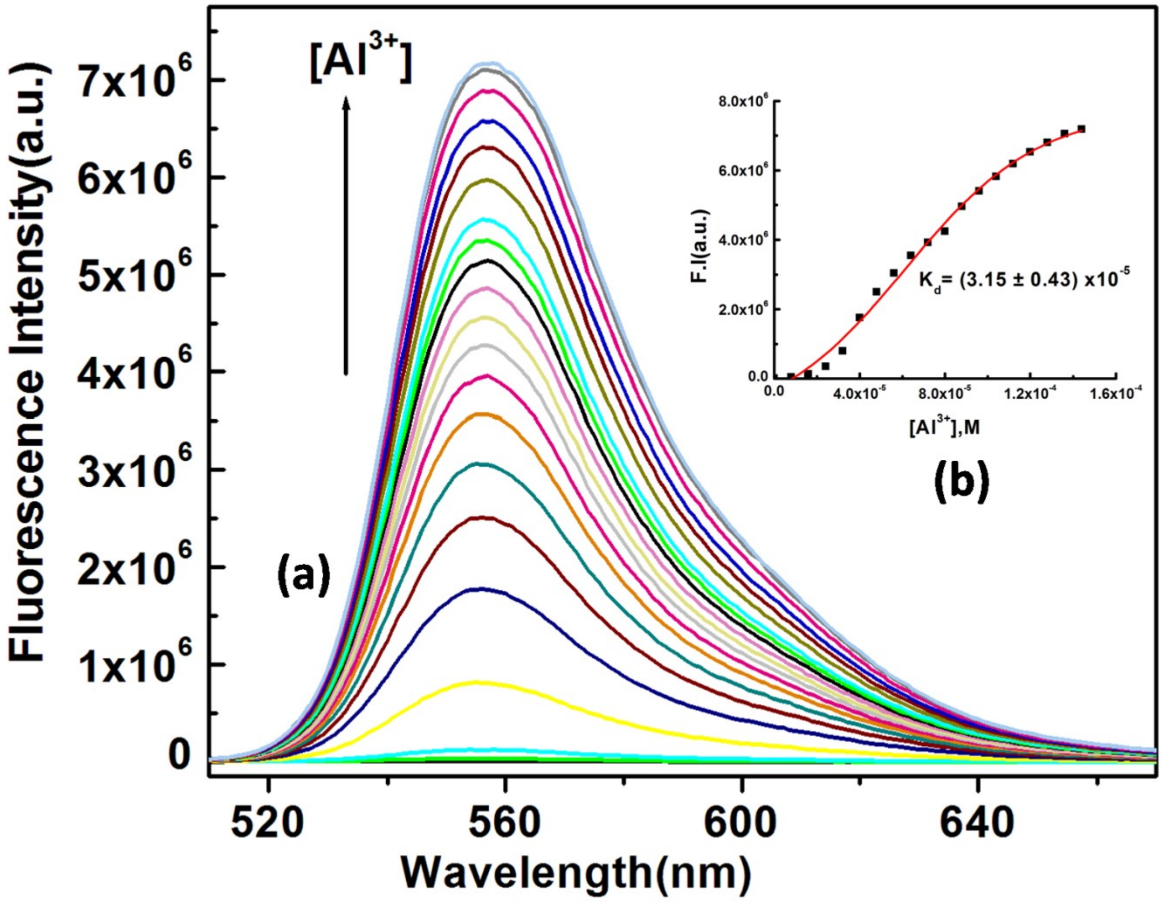

Fig. S6.(a) Fluorescence titration of **L^3**(60 μM) in H_2O- MeCN-(7:3, v/v) in HEPES buffer at pH 7.2 by the gradual addition of Al^{3+} (0-160 μM). Inset (b) Nonlinear curve-fit of F.I vs. [Al^{3+}] plot.

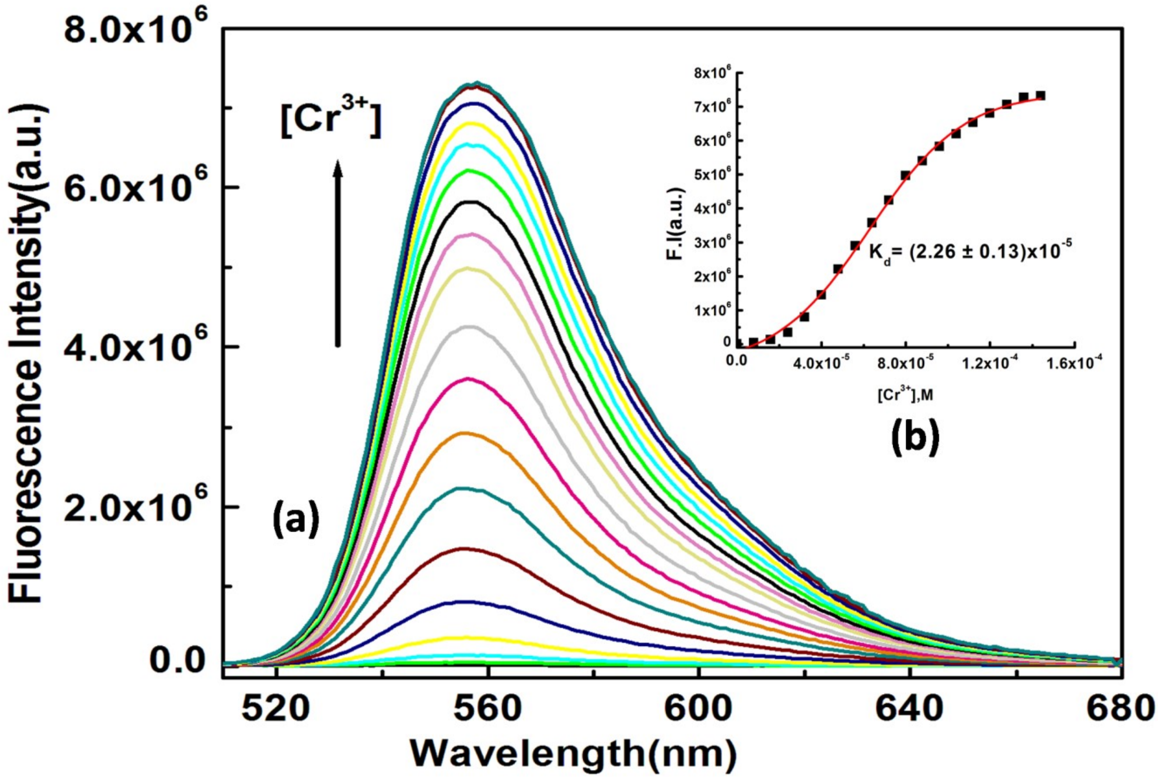

Fig.S6a.(a) Fluorometric titration of $\mathbf{L^3}$(60 μM) in H_2O- MeCN-(7:3, v/v) in HEPES buffer at pH 7.2 by the gradual addition of Cr^{3+} (0-160 μM). Inset (b) Nonlinear curve-fit of F.I vs. [Cr^{3+}] plot.

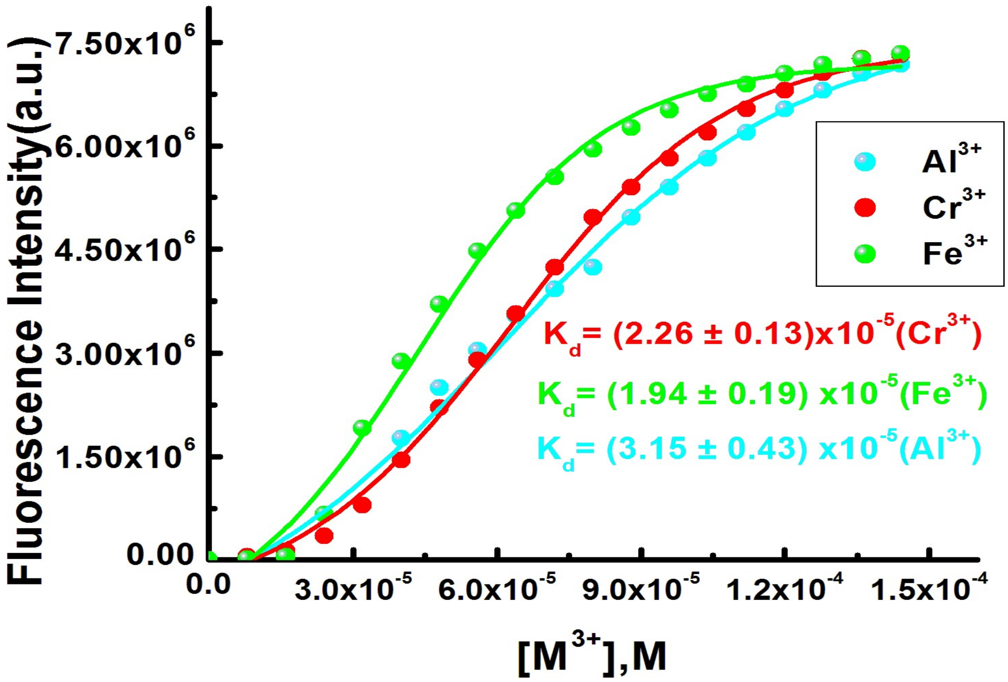

Fig.S6b. Non-linear fitting of fluorescence titration curves for Fe^{3+}, Al^{3+} and Cr^{3+} with K_d values.

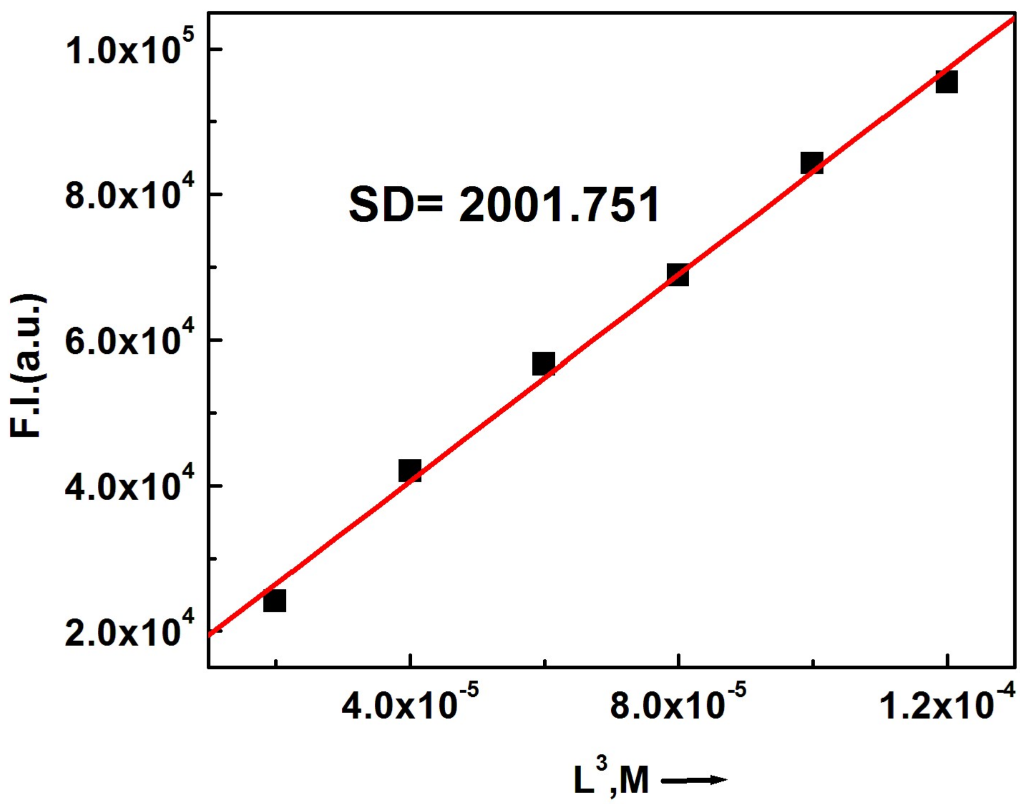

Fig. S7. Determination of S.D. of the blank, ligand(**L**^{3}) solution.

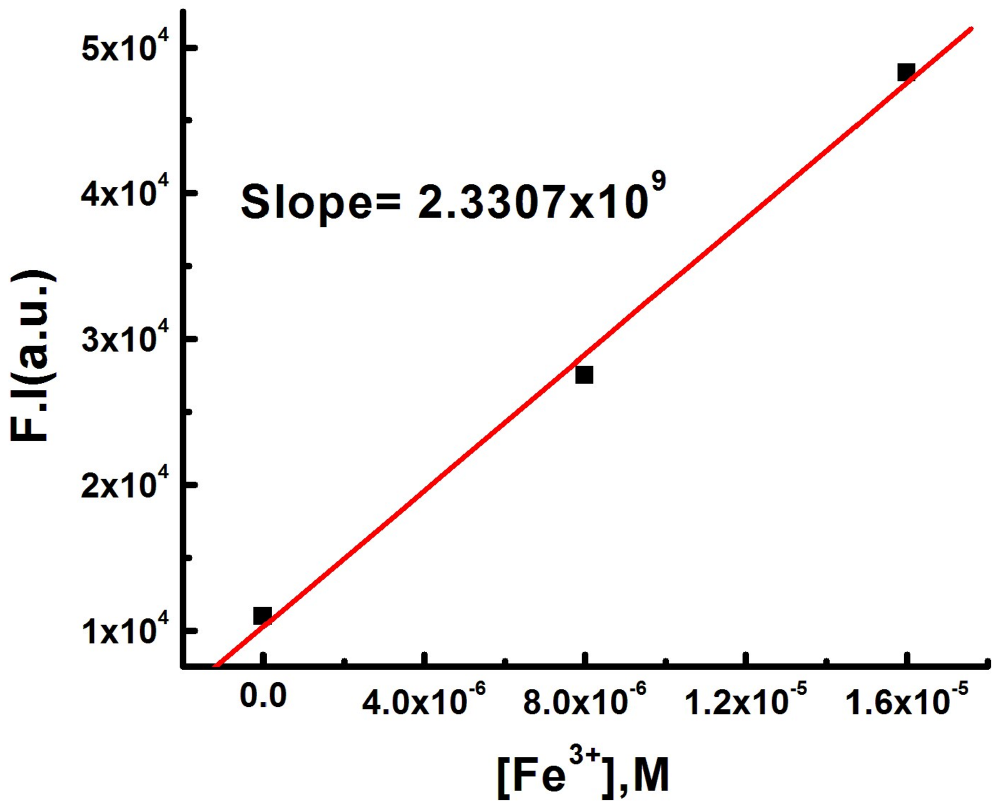

Fig.S8. Linear dyanamic plot of FI (at 558nm) vs [**Fe^{3+}**] for the determination of S (slope).

LOD(Fe^{3+}) = 3 x S.D/Slope

= (3 x 2001.751 /2.3307x10^9

= 2.57 μM

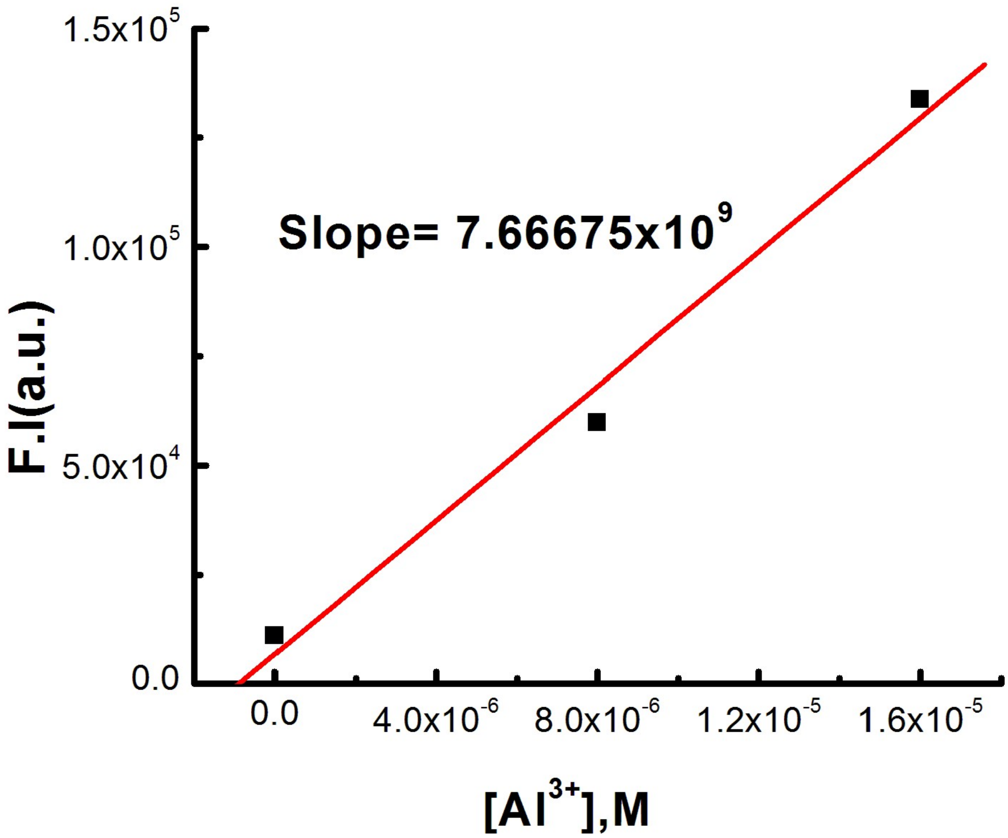

Fig.S8a. Linear dyanamic plot of FI (at 558nm) vs [Al^{3+}] for the determination of S (slope).

LOD(Al^{3+})= 3x S.D/Slope

= (3x 2001.751 /7.66675x10^9

= 0.78 μM

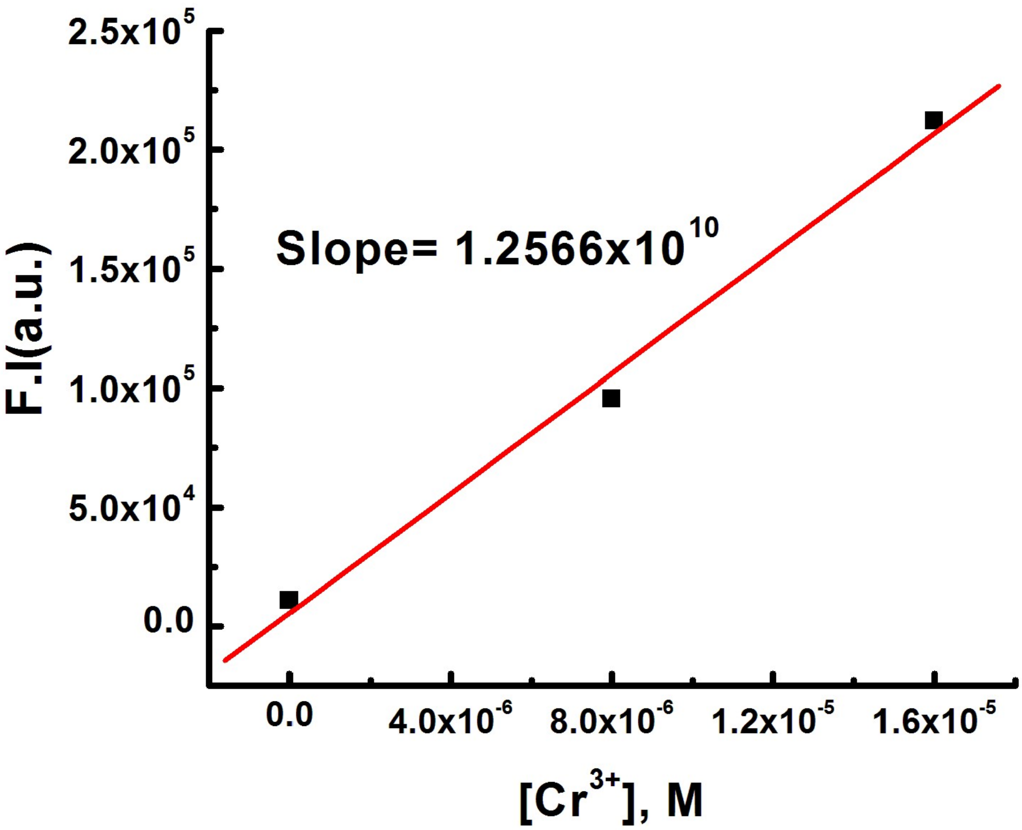

Fig.S8b. Linear dyanamic plot of FI (at 558nm) vs [**Cr^{3+}**] for the determination of S (slope).

LOD(Cr^{3+}) = 3 x S.D/Slope

= (3 x 2001.751 /1.2566x10^{10}

= 0.47 μM

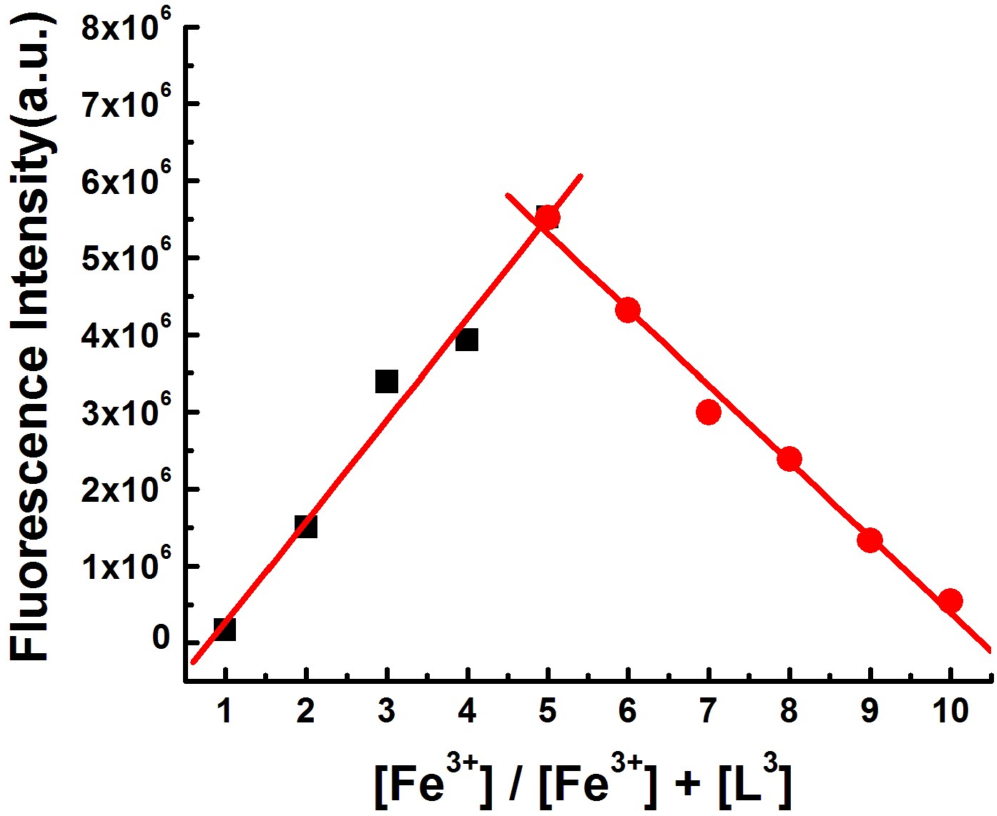

Fig. S9. Job's plot between **L**^{3}and Fe^{3+} for the confirmation of (1:1) binding.

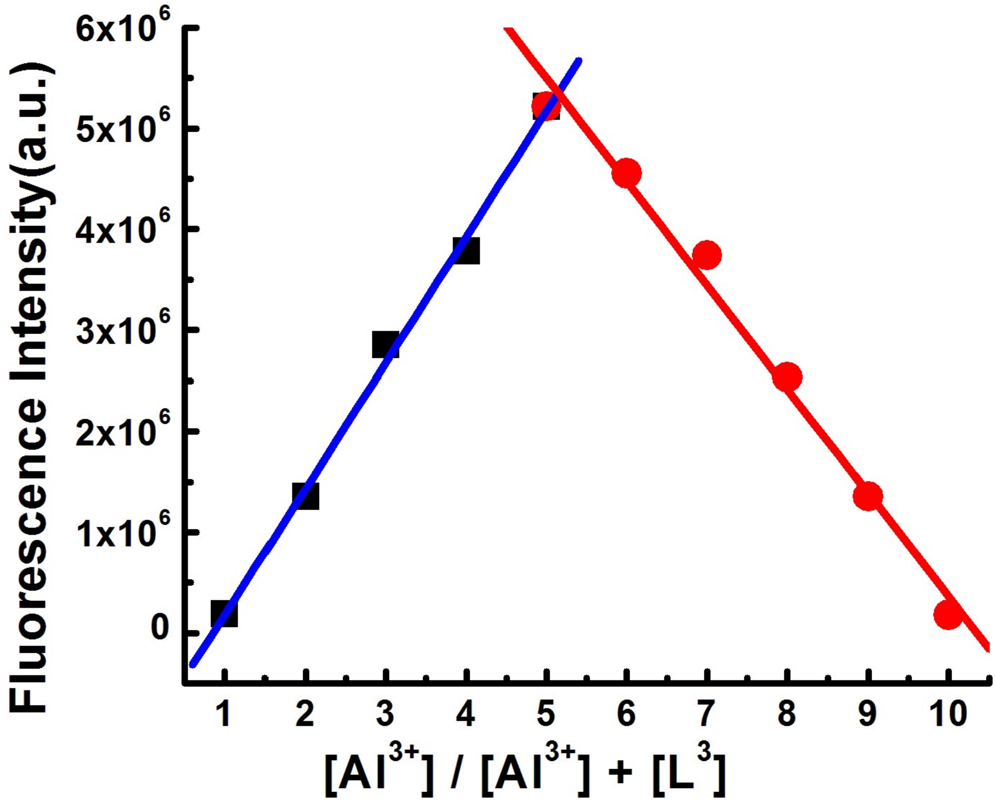

Fig. S9a. Job's plot between **L**^{3}and Al^{3+} for the confirmation of (1:1) binding.

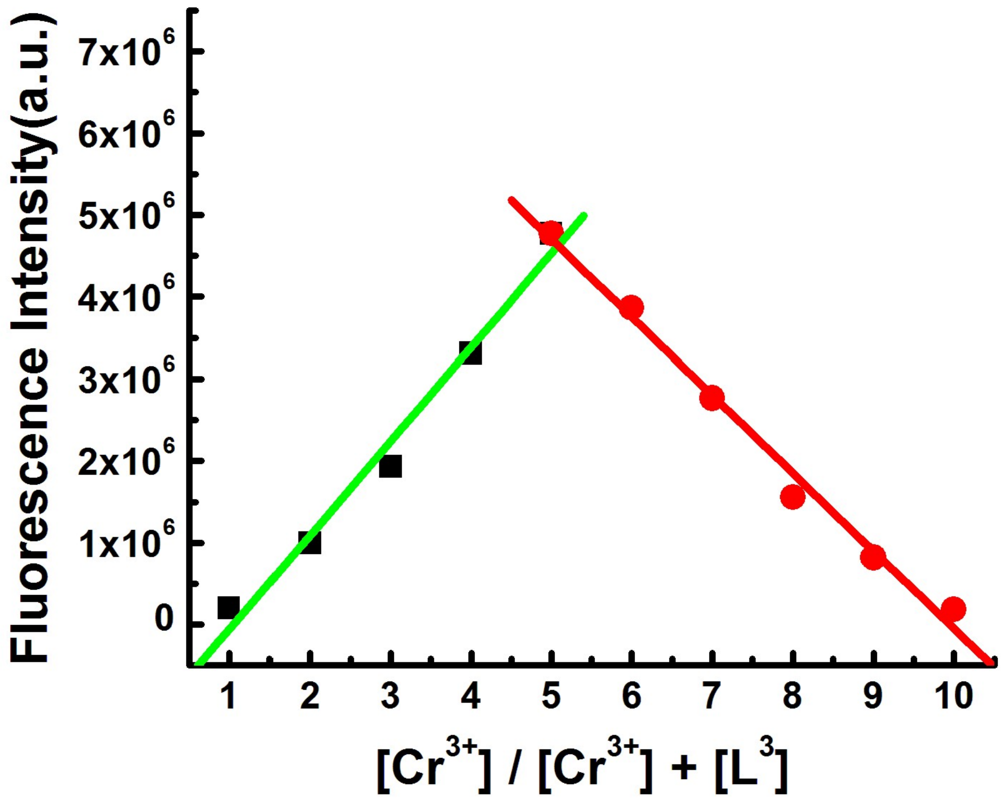

Fig. S9b. Job's plot between **L**^{3}and Cr^{3+} for the confirmation of (1:1) binding.

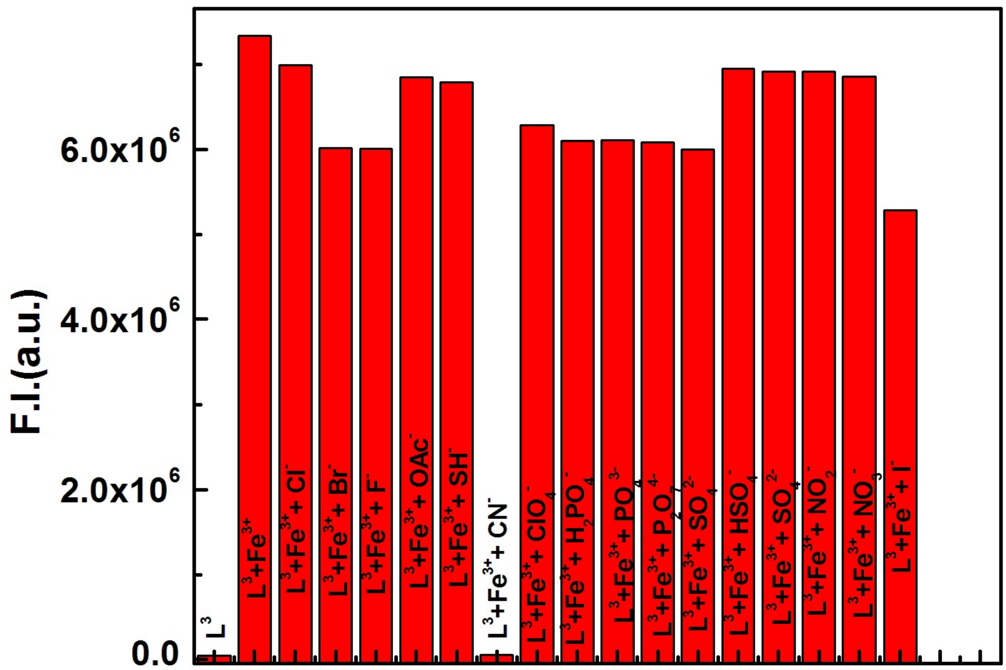

Fig. S10. Histogram of the fluorescence quenching [$\mathbf{L^3}$-Fe^{3+}]complex by CN^- (100 μM) towards $\mathbf{L^3}$ (60 μM) in H_2O- MeCN-(7:3, v/v) in presence of different anions(100μM) in HEPES buffer at pH 7.2 with λ_{ex} = 502 nm, λ_{em} = 558 nm.

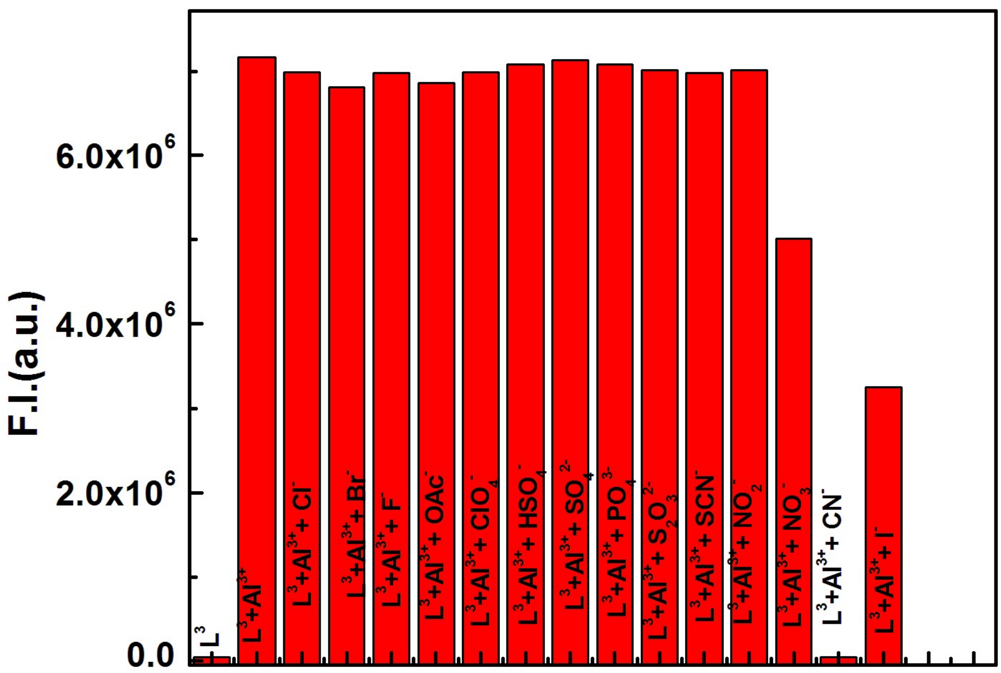

Fig. S10a. Histogram of the fluorescence quenching [$\mathbf{L^3}$-Al^{3+}]complex by CN^- (100 μM) towards $\mathbf{L^3}$ (60 μM) in H_2O- MeCN-(7:3, v/v) in presence of different anions(100μM)in HEPES buffer at pH 7.2 with λ_{ex} = 502 nm, λ_{em} = 558 nm.

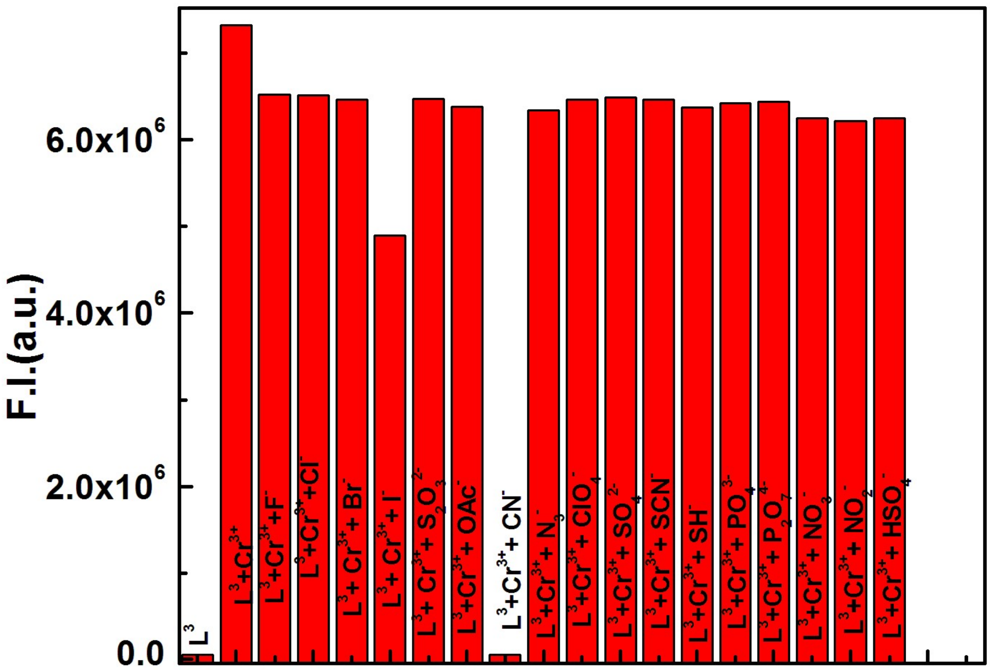

Fig. S10b. Histogram of the fluorescence quenching [**L**^{3}-Cr^{3+}]complex by CN^{-} (100 μM) towards **L**^{3} (60 μM) in H_2O- MeCN-(7:3, v/v) in presence of different anions(100μM) in HEPES buffer at pH 7.2 with λ_{ex} = 502 nm, λ_{em} = 558 nm.

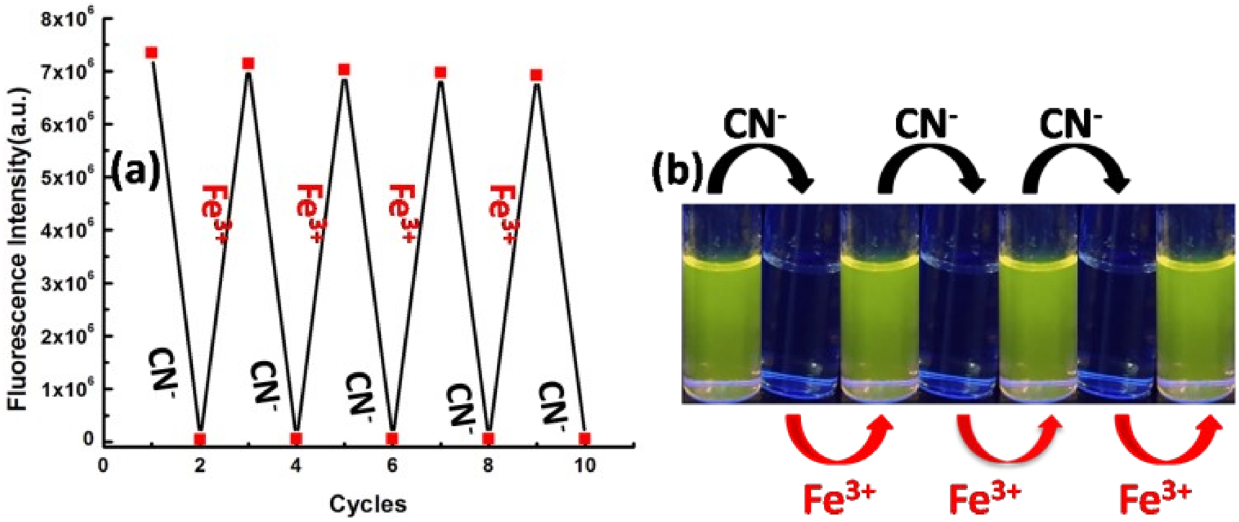

Fig.S10c. Fluorescence experiment to show the reversibility and reusability of the receptor for sensing $Fe^{3+}$by alternate addition of CN^{-}.(a) Fluorescence intensity obtained during the titration of **L**^{3}-$Fe^{3+}$with CN^{-} followed by the addition of Fe^{3+}. (b) Fluorescent color changes after each addition of CN^{-} and Fe^{3+} sequentially.

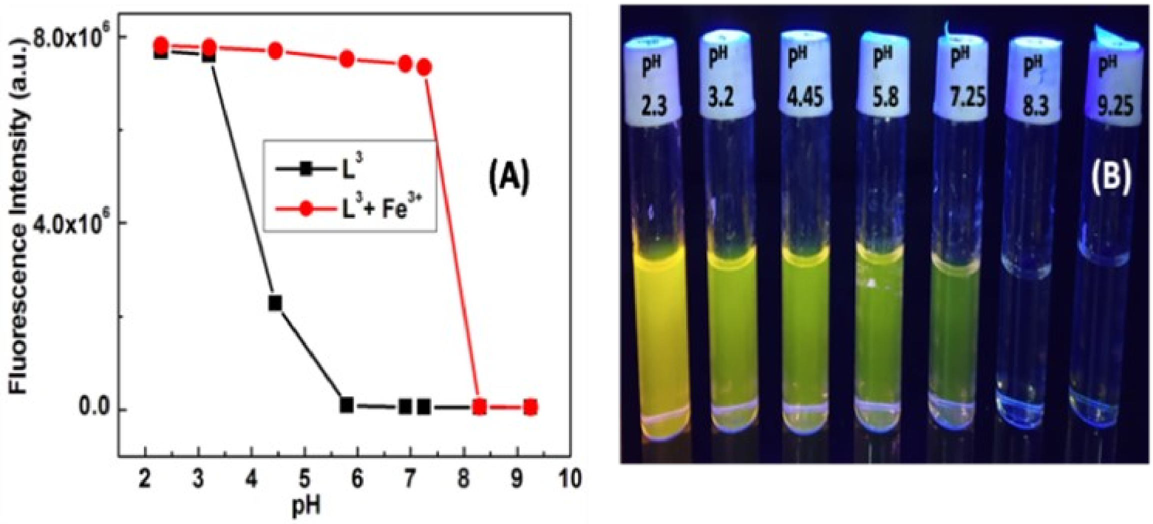

Fig.S11. (A) pH dependence of fluorescence responses of **L^3** and its **[L^3-Fe^{3+}]** complex; (B) Fluorescent response of **L^3** towards Fe^{3+} at different pH.

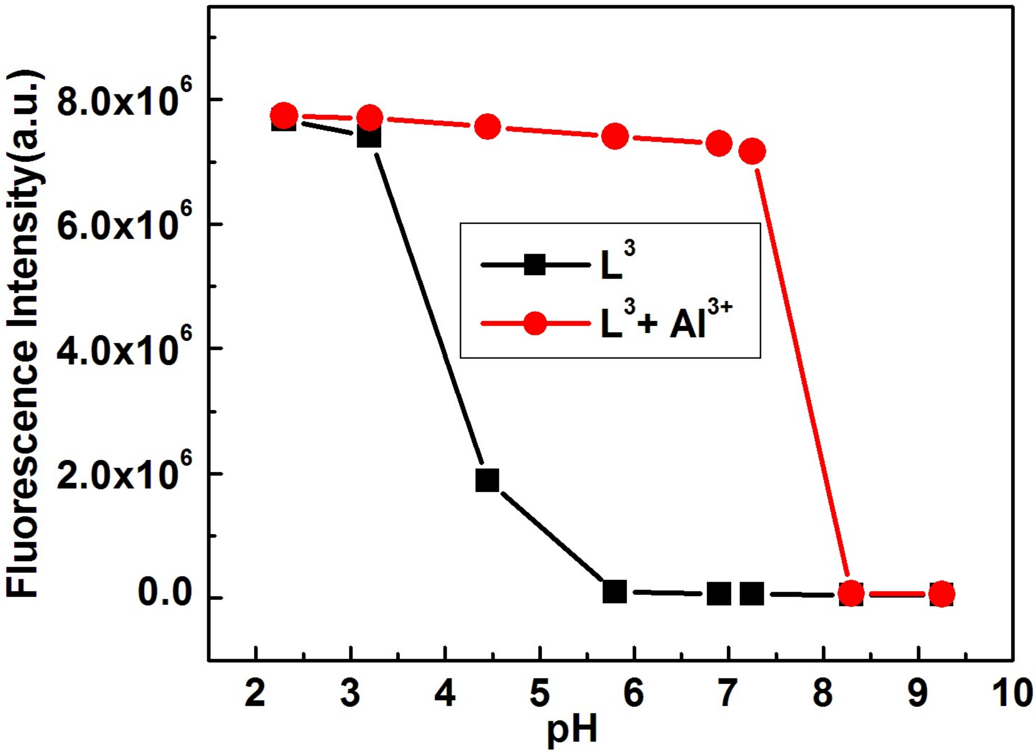

Fig. S11a. Fluorescence intensity observed at different pH for **L^3** and [**L^3**+Al^{3+}] (60 μM) in H_2O /CH_3CN (7:3,v/v) with λ_{ex} = 502 nm, λ_{em} = 558 nm.

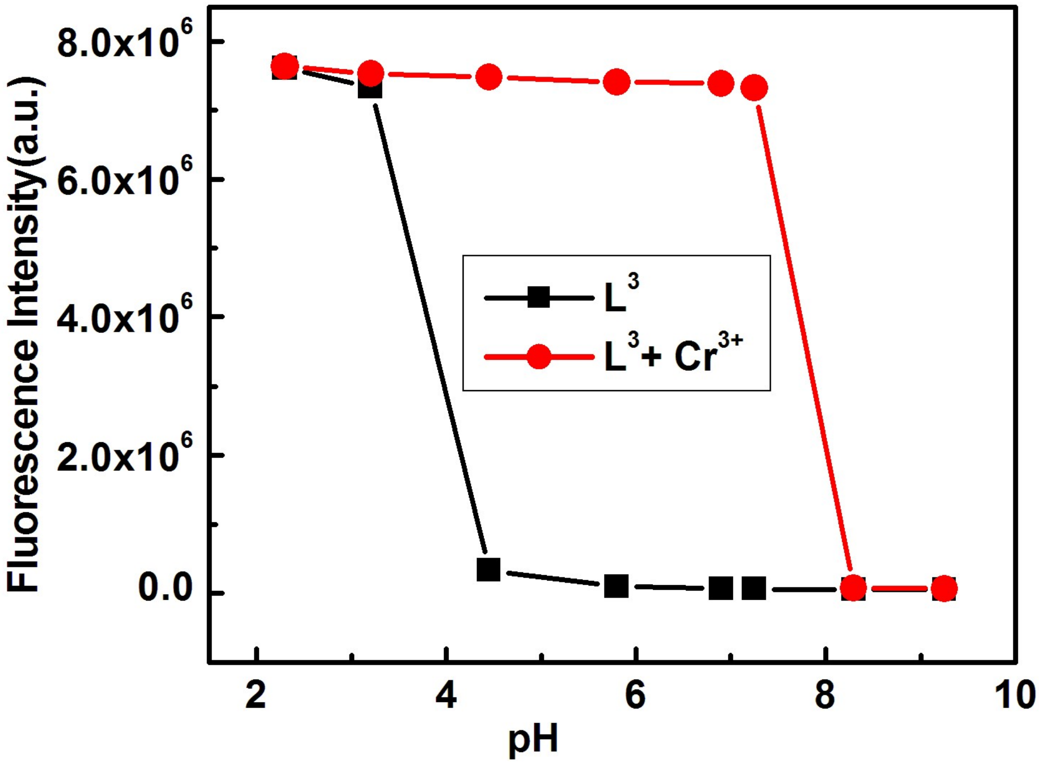

Fig. S11b. Fluorescence intensity observed at different pH for **L**^{3} and [**L**^{3}+Cr^{3+}] (60 μM) in H_2O /CH_3CN (7:3,v/v) with λ_{ex} = 502 nm, λ_{em} = 558 nm.

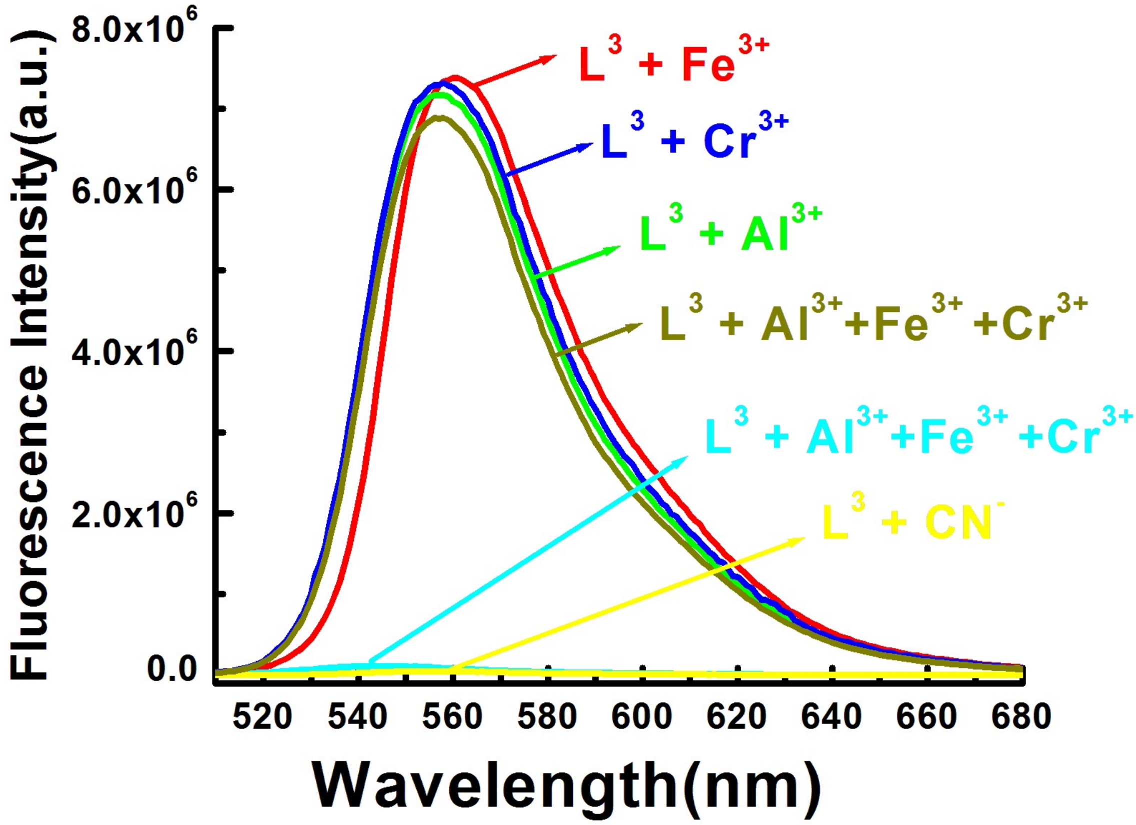

Fig. S12. Four-input OR-INHIBIT logic gate representation of the emission of $\mathbf{L^3}$ with different input when monitoring the emission at 558 nm.

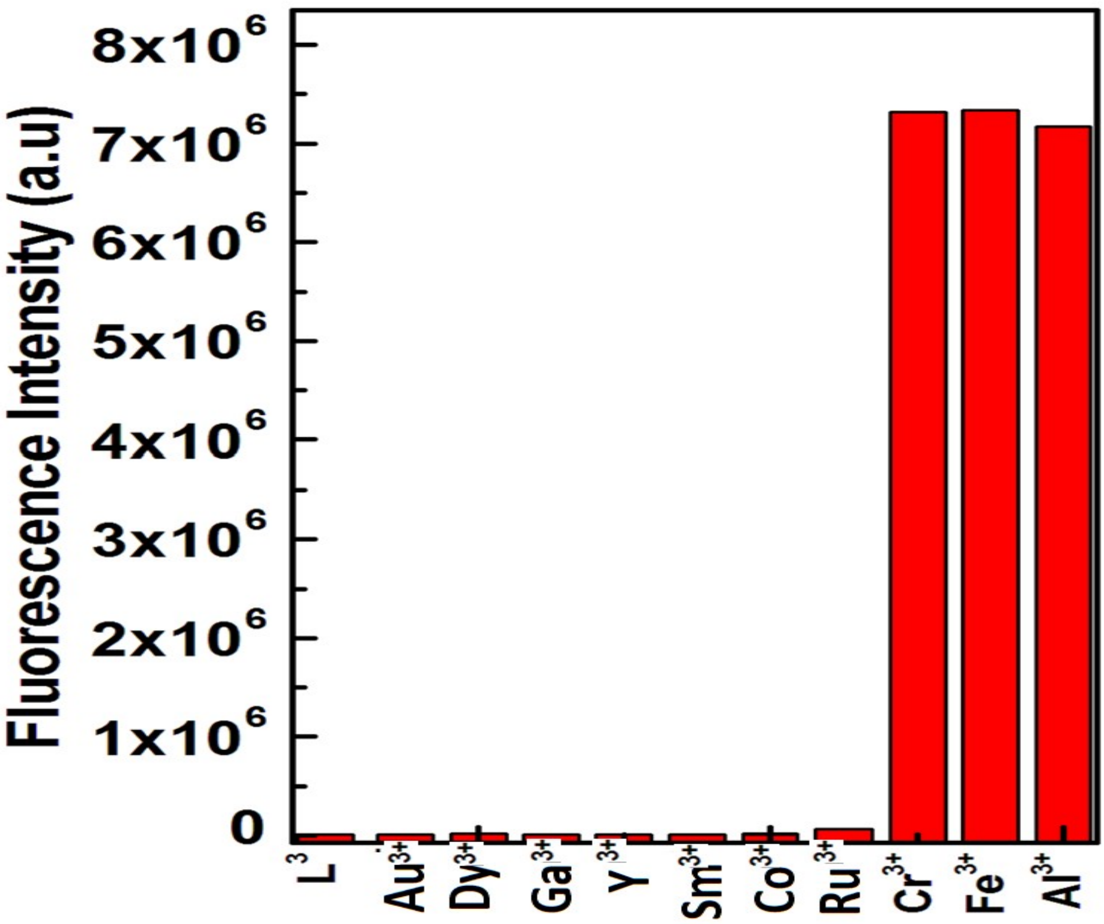

Fig. S13. Fluorescence response of the probe $\mathbf{L^3}$ in the presence of Au(III), Dy(III), Ga(III), Y(III), Sm(III), Ru(III) and Co(III) with respect to Fe^{3+}, Al^{3+} and Cr^{3+}

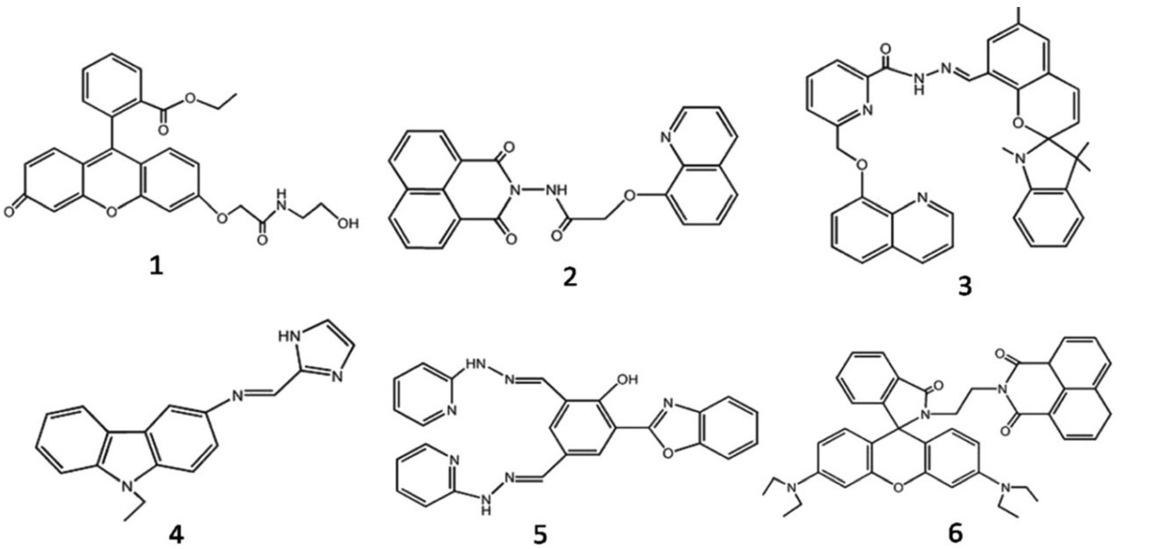

Fig. S14. Some previously representative trivalent sensors.

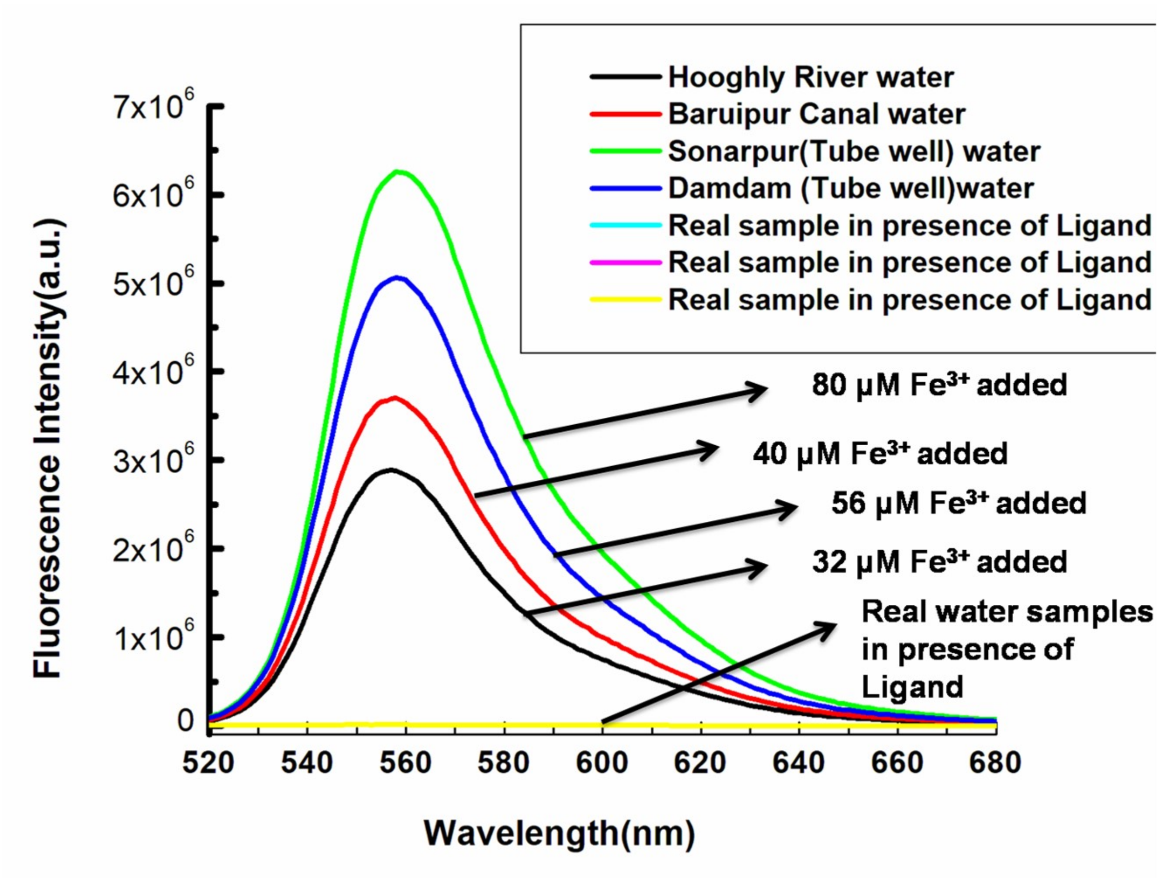

Fig. S15. Real water sample tested with the probe

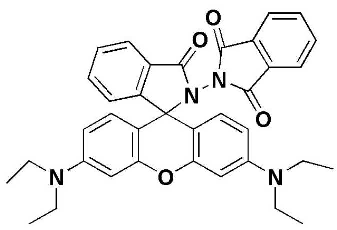

11

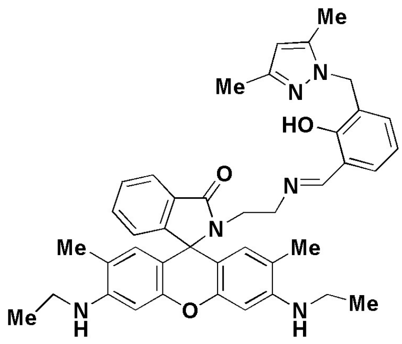

12

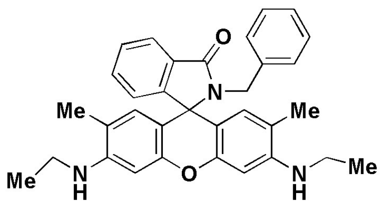

13

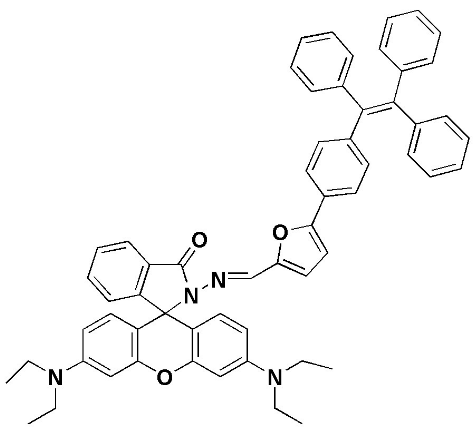

14

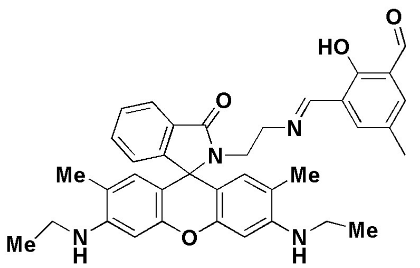

15

Fig. S16. Some previously reported rhodamine based trivalent sensors.

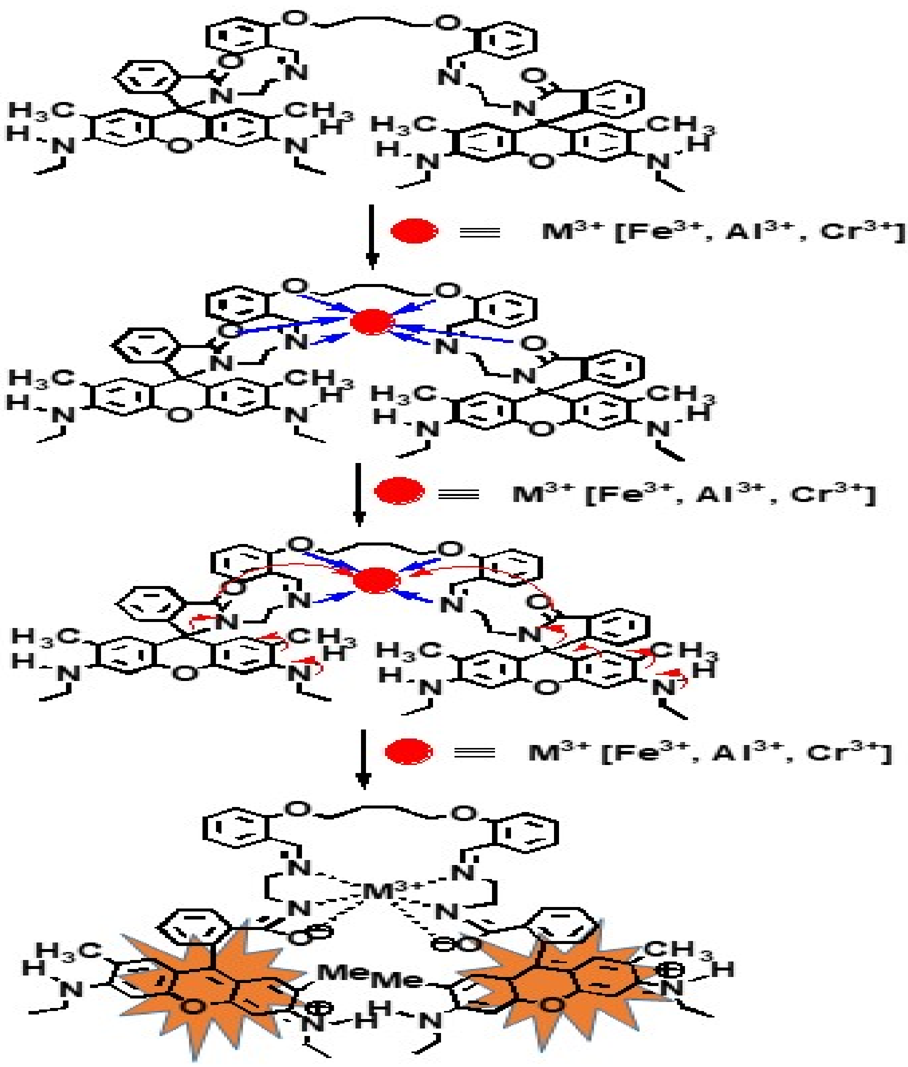

Scheme S1. Mechanism of spirolactum ring opening in the presence of M^{3+}(M=Fe, Cr, Al).

Table S1. A list of trivalent sensors along with some important parameters

Probe	Solvent	λ_{ex} (λ_{em})/ nm	LOD	K_f(M^{-1})	Ref no.
1	Pure CH_3CN	437(475)	0.5μM (Cr^{3+}) 0.3μM(Al^{3+}) 0.2μM(Fe^{3+})	1.58 x $10^4 M^{-1}$ (Cr^{3+}); 6.46 x 10^9 M^{-2} (Al^{3+}) 1.26 x 10^5 M^{-1} (Fe^{3+});	1
2	CH_3CN–HEPES buffer solution (40/60, v/v, pH = 7.4)	342 (484)	25μM(Cr^{3+}) 23μM(Al^{3+}) 20μM(Fe^{3+})	1.0852 x 10^4 M^{-1}(Fe^{3+}) 8.770 x 10^3 M^{-1} (Al^{3+}) 5.676 x 10^3 M^{-1}(Cr^{3+})	2
3	CH_3CN–HEPES buffer solution (1:1 , pH = 7.4)	460 (675)	93 nM(Cr^{3+}) 32 nM (Al^{3+}) 90 nM(Fe^{3+})	Not determined	3
4	THF–H_2O (8:2) mixture	330 (430)	0.36 nM (Cr^{3+}) 0.38 nM (Fe^{3+}) 0.38 nM (Al^{3+})	Not determined	4
5	H_2O:EtOH = 8:2	390(563) 390(527)	0.20μM(Cr^{3+}) 0.50μM(Al^{3+})	5.50 x 10^4 M^{-1} (Cr^{3+}) 2.00x 10^4 M^{-1} (Al^{3+});	5
6	CH_3OH–H_2O (6 : 4, v/v)	330(582)	1.74 nM (Al^{3+}) 2.36 μM (Cr^{3+}) 2.90 μM (Fe^{3+})	1 x 10^4 M^{-1} (Al^{3+}); 2.6 x 10^2 M^{-1} (Cr^{3+}) 1.2 x 10^2 M^{-1} (Fe^{3+});	6
7	CH_3CN	Colorimetric	2.16 × 10^{-6} M(Al^{3+}) 1.27 × 10^{-8} M(Cr^{3+}) 5.03 × 10^{-8}M(Fe^{3+})	3.451 × $10^3 M^{-1}$(Al^{3+}) 3.751 × 10^6 M^{-1}(Cr^{3+}) 6.078 × 10^6 M^{-1}(Fe^{3+})	7
8	Methanol:water (7:3, v/v)	500(552)	1.18nM(Al^{3+}) 1.80nM(Cr^{3+}) 4.04 nM(Fe^{3+})	6.92 ± 0.18μM (Al^{3+}) 4.90 ± 0.67 μM (Fe^{3+}) 6.79 ± 0.34 μM (Cr^{3+})	8
9	1:1 methanol–water	365(509)	1.6×10^{-6} M(Al^{3+}) 2.66×10^{-6}M(Cr^{3+}) 7.99×10^{-7}M(Fe^{3+})	Not determined	9
10	CH_3CN	365(465)	1.06 × 10^{-7}M(Fe^{3+}) 1.11 × 10^{-7}M(Cr^{3+}) 1.17 × 10^{-7}M(Al^{3+})	2.25 × $10^6 M^{-2}$(Fe^{3+}) 2.24 × $10^6 M^{-2}$(Cr^{3+}) 2.26 × $10^6 M^{-2}$(Al^{3+})	10

Table S2. A list rhodamine based trivalent sensors along with some important parameters

Probe	Solvent	λ_{ex} (λ_{em})/ nm	LOD	K_f (M^{-1})	Ref no.
11	CH_3CN: Tris-buffer(1:1, v/v)	520(586)	1.10 × 10^{-5} M(Fe^{3+}) 3.20 × 10^{-7} M(Al^{3+}) 2.55 × 10^{-5} M(Cr^{3+})	6.13 x 10^4 M^{-1}(Fe^{3+}) 3.14 x 10^3 M^{-1} (Al^{3+}) 2.26 x 10^3 M^{-1}(Cr^{3+})	11
12	methanol/H_2O (1:1, v/v,)	510(555)	0.29mM (Fe^{3+}) 0.34mM (Al^{3+}) 0.31 mM (Cr^{3+})	6.7 x 10^4 M^{-1}(Fe^{3+}) 8.2 x 10^4 M^{-1} (Al^{3+}) 6.0 x 10^4 M^{-1}(Cr^{3+})	12
13	H_2O/CH_3CN (4:1, v/v)	502(558)	1.28 μM (Fe^{3+}) 1.34 μM (Al^{3+}) 2.28 μM (Cr^{3+})	9.4 x 10^3 M^{-1}(Fe^{3+}) 1.34 x 10^4 M^{-1} (Al^{3+}) 8.37 x 10^3 M^{-1}(Cr^{3+})	13
14	CH_3CN–H_2O (3:2, v/v)	520(582)	3.2 μM (Fe^{3+}) 4.8 μM (Al^{3+}) 0.93 μM (Cr^{3+})	Not determined	14
15	Methanol:water (9:1, v/v)	500(550)	14.0 nM (Fe^{3+}) 15.80 μM (Al^{3+}) 0.93 μM (Cr^{3+})	8.74 × 10^4(Fe^{3+}) 6.24 × 10^4(Cr^{3+}) 1.47 × 10^5(Al^{3+})	15
16	H_2O/CH_3CN (7:3, v/v, pH 7.2, 20 mM HEPES buffer	502(558)	2.57μM (Fe^{3+}) 0.78 μM(Al^{3+}) 0.47 μM(Cr^{3+})	5.15x10^4 M^{-1} (Fe^{3+}) 3.17 x 10^4 M^{-1}(Al^{3+}) 4.42 x 10^5 M^{-1}(Cr^{3+})	In this work

Table S3. Determination of Fe^{3+} concentrations in real water samples.

Place	Fe^{3+} added(μM)	Fe^{3+} found(μM)
Hooghly River water	32	32.08
Baruipur canal water	40	40.12
Sonarpur (tube well water)	56	56.37
Damdam (tube well water)	80	80.59

References

1. A. Barba-Bon, A.M.Costero, S.Gil, M. Parra, J. Soto, R. Martínez-Má-ñez and F. Sancenón, *Chem. Commun*., 2012, **48**, 3000.
2. S. Goswami, K. Aich, A. K. Das, A. Manna and S. Das, *RSC Advances*, 2013, **3**, 2412.
3. S. Goswami, K. Aich, S. Das, A. K. Das, D. Sarkar, S. Panja, T. K.Mondal and S. Mukhopadhyay, *Chem. Commun.,* 2013, **49**, 10739.

4. M. Venkateswarulu, T. Mukherjee, S. Mukherjee and R. R.Koner, *Dalton Trans*., 2014, **43**, 5269.
5. J. Wang,Y. Li,N. G. Patel, G. Zhang, D. Zhou and Y. Pang, *Chem. Commun*., 2014, **50**, 12258.
6. S. Paul, A. Manna and S. Goswami, *Dalton Trans*., 2015, **44**,11805.
7. P. N. Borase, P. B. Thale, S. K. Sahoo and G.S. Shankarling, *Sensors and Actuators B*, 2015, **215**, 451.
8. S. Dey, S. Sarkar, D. Maity and P. Roy, *Sensors and Actuators B*, 2017, **246**, 518.
9. S. Samanta, S. Goswami, A. Ramesh and G. Das, *Sensors and Actuators B*, 2014, **194**,120.
10. T. Simon, M. Shellaiah, V. Srinivasadesikan, C.-C. Lin, F. -H. Ko, K. Wen Sun and M.-C. Lin, *Sensors and Actuators B*, 2016, **23**,18.
11. X. Wan, T. Liu, H. Liu,L. Gu, Y. Yao,RSC Adv., 2014,**4**, 29479
12. R. Alam, R. Bhowmick, A.S.M. Islam, A.katarkar, K.Chaudhurib and M. Ali, New J. Chem.,2017, **41**, 8359.
13. D. Das, R. Alam, A. Katarkar and M. Ali Photochem. Photobiol. Sci., 2019, **18**, 242.
14. H.X. Yu, J. Zhi, Z.F. Chang, T.Shen, W.L.Ding, X. Zhang and J.L. Wang, Mater. Chem. Front., 2019, **3**, 151
15. A. Roy, S. Das, S. Sacher, S. K. Mandal and P. Roy, Dalton Trans., 2019, **48**, 17594.